THE JOURNAL OF PHYSICAL CHEMISTRY A

Article

Decoding the Dynamical Information Embedded in Highly Excited Vibrational Eigenstates: State Space and Phase Space Viewpoints

Paranjothy Manikandan, Aravindan Semparithi, and Srihari Keshavamurthy

J. Phys. Chem. A, **2009**, 113 (9), 1717-1730• DOI: 10.1021/jp807231p • Publication Date (Web): 11 February 2009

Decoding the Dynamical Information Embedded in Highly Excited Vibrational Eigenstates: State Space and Phase Space Viewpoints

Paranjothy Manikandan, Aravindan Semparithi,[†] and Srihari Keshavamurthy*

Department of Chemistry, Indian Institute of Technology, Kanpur, Uttar Pradesh 208016, India

Received: August 13, 2008; Revised Manuscript Received: January 6, 2009

We study the nature of highly excited eigenstates of strongly coupled multimode systems with three degrees of freedom. Attempts to dynamically assign the eigenstates using classical-quantum correspondence techniques poses a considerable challenge, due to both the number of degrees of freedom and the extensive chaos in the underlying classical phase space. Nevertheless, we show that sequences of localized states interspersed between delocalized states can be identified readily by using the parametric variation technique proposed earlier by us. In addition, we introduce a novel method to lift the quantum eigenstates onto the classical resonance web using a wavelet-based local time−frequency approach. It is shown that the lifting procedure provides clear information on the various dominant nonlinear resonances that influence the eigenstates. Analyzing the spectroscopic Hamiltonians for CDBrClF and CF_3CHFI as examples, we illustrate our approach and demonstrate the consistency between state space and phase space perspectives of the eigenstates. Two exemplary cases of highly mixed quantum states are discussed to highlight the difficulties associated with their assignment. In particular, we provide arguments to distinguish between the states in terms of their predominantly classical or quantum nature of the mixing.

1. Introduction

Several groups, over studies spanning nearly three decades, have established that decoding the dynamical information hidden in highly excited quantum states is best done via the classical-quantum approach.[1−24] In other words, the assignments are based on invariant classical phase space structures and there is sufficient evidence that changes in the phase space structures translate into appearance/disappearance of new classes of quantum eigenstates as well as spectral perturbations.[1,5,18] For example, the celebrated Einstein−Brillouin−Keller (EBK) method[21] utilizes the phase space tori for assignment in the integrable case. At the other extreme of strongly chaotic phase spaces one has quantization based on periodic orbits and the scarring[22] of quantum states by the unstable periodic orbits. Thanks to the finiteness of the Planck's constant, it is even possible to assign quantum states based on partial structures in the phase space like vague tori[23] and recent studies[24] have also established the crucial role played by the homoclinic orbits. At the same time, rapid developements[25] in our ability to calculate accurate rovibrational eigenstates and eigenvalues provide a unique opportunity to critically examine and extend the methods based on classical-quantum correspondence to systems with a large number of degrees of freedom.

The importance of such studies stems from the fact that the structure and patterns exhibited by the highly excited eigenstates yields valuable insights into the process of intramolecular vibrational energy redistribution (IVR)[26−30] which, in turn, leads to a better understanding of chemical reaction dynamics. Although IVR is understood more naturally from a time-dependent viewpoint, i.e., the dynamics of a zeroth-order bright state and its mixing with the zeroth-order dark states belonging to different tiers,[26] the time-independent perspective has its own merits. The apparent contradiction, that a molecular eigenstate does not "move" and hence there is no IVR, is easily resolved since the natural representation is now the energy or frequency domain. Therefore the infinite time limit of the IVR dynamics is imprinted onto the eigenstates in the form of subtle features, both strong and weak.[27] The time and frequency domain information are Fourier related and, hence, it is possible to infer the time-dependent dynamics from the fractionation pattern of a bright state as revealed by a frequency domain experiment. In this sense, assignment of the highly excited eigenstates is tantamount to insights into the IVR dynamics of the molecule.

Assigning the eigenstate, at any energy, of a molecule with D vibrational degrees of freedom means that one can associate D good quantum numbers with the state. The existence of such a set of quantum numbers associated with D mutually commuting set of operators is, however, very rare in generic systems. At energies close to equilibrium, eigenstates can be assigned, assuming the absence of phenomenon like monodromy[31] and dynamical tunneling,[32,33] in terms of uncoupled harmonic oscillators (normal modes) or uncoupled Morse oscillators (local modes). The situation is more complicated at higher energies due to the coupling of the normal (local) modes, and it is not possible to guarantee the existence of the required number of good quantum numbers. Needless to say, the energy at which mixed states begin to show up is strongly dependent on the size of the molecule; for large molecules highly mixed states can be observed already around energies corresponding to the first vibrational overtone. On the other hand, highly vibrationally excited states of small molecules are expected to be significantly mixed.

The essence of any method for dynamical assignment of eigenstates is to identify the part of the phase space supporting localized eigenstates. If the dynamical nature of that part of the phase space can be identified, then hopefully a sequence of eigenstates can be found. The organization of the sequence of eigenstates can than be naturally ascribed to the existence of

* Corresponding author.
[†] Current address: Institut Charles Gerhardt (CTMM), CC 1501, Universite Montpellier II−CNRS, 34095 Montpellier, Cedex 05, France.

10.1021/jp807231p CCC: $40.75
Published on Web 02/11/2009

some approximate conserved quantities implying the existence of approximate quantum numbers. One can debate the utility of a level-by-level assignment of molecular eigenstates as opposed to a global statistical description.[34,35] In this regard we note that molecular systems rarely, if ever, approach the random matrix limit. Moreover, even for a molecule with large density of states, one might be interested in a select group of eigenstates, in some energy range of interest, whose assignment leads to insights into the dynamics of the molecule.[36−38] For instance, a recent investigation of conformational isomerization reaction clearly highlights the link between deviations from statisticality and the existence of several classes of vibrational eigenstates.[37]

However, the dynamical assignment approach runs into severe difficulties for systems with three or more degrees of freedom. The reasons for the difficulties are well documented in the literature, and we refer the reader to the earlier works for a detailed exposition.[4] In short, low dimensional approaches cannot be extended in a straightforward fashion and there is a need for alternative ways of extracting the dynamical information encoded in the mixed quantum states. The present work, motivated by the usefulness of the dynamical assignment, focuses on analyzing the highly excited eigenstates of systems with three degrees of freedom in order to alleviate some of the inherent difficulties associated with the classical-quantum correspondence approach for such systems. Several different tools are used to elucidate the nature of the highly excited eigenstates. In particular, a new method for lifting the eigenstates onto an appropriate representation of the phase space is proposed. We show that a combination of techniques can efficiently reveal the localized eigenstates interspersed among the highly mixed ones and further distinguish between mixed states arising due to predominantly classical or quantum mechanisms.

We start with the theoretical background for dynamical assignments, followed by a description of the methods used in the current work. In the subsequent sections we illustrate our approach using the spectroscopic Hamiltonians for CDBrClF[29] and CF_3CHFI[30] as examples. The choice of these systems is motivated by the pioneering experimental and theoretical studies[28] of CD/CH chromophore dynamics by Quack and coworkers. Apart from elucidating several features of the IVR dynamics in these systems, such studies have provided explicit effective Hamiltonians for analyzing the dynamics and eigenstates in specific energy regimes. Further motivation comes from recent detailed studies[7,8] by Jung et al. on the same systems as above wherein insights into the nature of the eigenstates and their dynamical assignments are provided. In the systems of interest for the current study, the Hamiltonians involve four strongly coupled high-frequency modes with a conserved polyad. Thus, despite having effectively three degrees of freedom, both systems possess many highly mixed quantum states due to the presence of strong anharmonic resonances. Hence, the examples considered in the current work provide a stringent test for any classical-quantum correspondence based analysis. The last section concludes with remarks and future outlook.

2. Theoretical Background

2.1. Hamiltonian. In this study we focus on spectroscopic Hamiltonians for vibrations which can be expressed as

$$H = H_0 + \sum_k \tau_k V_k(\mathbf{a}, \mathbf{a}^\dagger) \tag{1}$$

with the zeroth-order Dunham term[39]

$$H_0 = \sum_{j=1}^{N} \omega_j v_j + \sum_{i,j=1}^{N} x_{ij} v_i v_j + \ldots \tag{2}$$

In the above equations, a_j, $a_j^\dagger$, and $v_j \equiv a_j^\dagger a_j$ are the harmonic destruction, creation, and number operators of the jth-mode respectively. The harmonic frequencies and anharmonicities are denoted by ω_j and x_{ij}, respectively. We make two observations at this stage. First, the Dunham expansion can be carried out to higher order in anharmonicities and inclusion of the higher order terms is not a constraining factor for the method proposed in this work. Second, as opposed to the above normal-mode basis, one can use a local-mode basis leading to the so-called algebraic Hamiltonians.[19] Although the classical limit Hamiltonian is more complicated in such cases, the analysis presented here can be done with no additional complications. We also note that the advantages and disadvantages of using a spectroscopic Hamiltonian are well-known and hence will not be reiterated here. It is useful to mention, however, that the dynamics inferred from the analysis is on a firmer basis if the spectroscopic Hamiltonian is extracted[9,40,41] from a global potential energy surface by performing a quantum Van Vleck[42] or classical Birkhoff−Gustavson perturbation[43,44] theory.

In eq 1 the various anharmonic resonances

$$V_k = \prod_{j=1}^{N} (a_j^\dagger)^{m_{jk}^+} (a_j)^{m_{jk}^-} + \text{h.c} \tag{3}$$

with $m_k \equiv (m_{1k}^{\pm}, m_{2k}^{\pm}, \cdots, m_{Nk}^{\pm})$ are necessary to obtain an accurate description of the vibrational eigenstates and dynamics. Note that we are assuming the Hamiltonian to be already in the simplest form possible taking into account the various conserved quantities[45,46] (polyads) $\mathbf{K} \equiv (K_1, \cdots, K_F)$. Thus, the original system has the full dimensionality $D = N + F$ and an effective dimensionality $N < D$. The existence and construction of the polyads are well understood and related to the nature and number of independent resonances among the D vibrational modes.[45,46] Typically, some (or all) of the polyads might be approximate depending on the energy range of interest since eq 1 often ignores other smaller perturbations. The extent to which specific polyads are conserved is also evident from the experimental spectra. Indeed, the concept of polyads plays a crucial role in interpreting the various spectral features.[47]

2.2. Need for Dynamical Assignments. Clearly, with no further information, all eigenstates can be assigned F quantum numbers corresponding to the polyads. A complete assignment would require specifying the remaining $(D - F)$ quantum numbers. Strictly speaking, in generic systems, finding the remaining quantum numbers is a hopeless task since they do not exist. Nevertheless, for a given set $(K_1, \cdots, K_F)$ certain eigenstates might be predominantly influenced by a few, single, or none of the resonances. In such instances the eigenstates are localized and characterized by an appropriate number of quantum numbers. The additional, necessarily approximate, quantum numbers can be thought of as arising from the approximate decomposition of a polyad into subpolyads, for example, $K_j \approx \tilde{K}_1 + \tilde{K}_2 + \tilde{K}_3$. It is important to realize that the origin of the subpolyads $\tilde{\mathbf{K}}$ is dynamical, i.e., the approximate decomposition (or decoupling) is a consequence of the dynamics. Therefore the possible $\tilde{\mathbf{K}}$ are not easily determined by the inspection of the Hamiltonian or even the experimental spectrum alone. A more detailed discussion of the notion of approximate conserved quantities and their impact on IVR can be found in the article by Kuzmin and Stuchebrukhov.[48] Further, in a given energy range it is quite possible for different dynamical decouplings to manifest resulting in a complicated interleaving

pattern of localized eigenstates. From the above discussion it is clear that a dynamical assignment of the eigenstates is the correct approach to adopt. An added bonus is that the dynamical assignment automatically reveals the dynamics encoded in a given quantum state.

The essential idea is that regions in the classical phase space which are characterized by smaller than average classical instability may trap classical trajectories. In the context of the Hamiltonian above, such traps can be due to the dominance of a particular resonance and it is expected that this leads to long time dynamical correlations. The resulting phase space inhomogeneity, in turn, can give rise to wave function localization. Therefore the first step in the analysis is to study the dynamics of the classical limit Hamiltonian corresponding to eq 1. Transition to the classical limit is particularly simple for spectroscopic Hamiltonians (obtained via the correspondence principle)[49] and the resulting classical Hamiltonian can be written as

$$\mathscr{H}(\mathbf{J}, \boldsymbol{\psi}) = \mathscr{H}_0(\mathbf{J}) + 2\sum_k \tau_k f_k(\mathbf{J}) \cos(\mathbf{m}_k \cdot \boldsymbol{\psi}) \qquad (4)$$

The action-angle variables[50] $(\mathbf{J}, \boldsymbol{\psi})$ in eq 4 are related to the original action-angle variables $(\mathbf{I}, \boldsymbol{\phi}) \equiv (I_1, \cdots, I_D, \phi_1, \cdots, \phi_D)$ of the unperturbed part of the D-dimensional Hamiltonian via a canonical transformation. The canonical transformation leads to explicit reduction of the system to N-degrees of freedom and thus $(\mathbf{J}, \boldsymbol{\psi}) \equiv (J_1, \cdots, J_N, \psi_1, \cdots, \psi_N)$. The reduced Hamiltonian is cyclic in the remaining angle variables $(\psi_{N+1}, \cdots, \psi_{N+F})$ which are conjugate to the classically conserved quantities $\{K_j^c; j = N+1, \cdots, N+F\}$. Thus, $\mathbf{K}^c$ are the classical analog to the quantum polyads $\mathbf{K}$. The various anharmonic resonances in eq 1 manifest as nonlinear resonances in eq 4. For systems with $N = 2$ there are a number of techniques that can be utilized to dynamically assign the quantum states[34,35,3,14,16,13] On the other hand, for systems with $N \geq 3$ very few approaches are avaliable[7−11] and have to do with the fact that most of the methods used in $N = 2$ are difficult, if not impossible, to generalize.[4]

2.3. Semiclassical Wave Function Approach. A first step toward extending the classical quantum based dynamical assignments for $N \geq 3$ was taken recently by Jung et al. in a series of papers.[7−9] Their approach, inspired by an earlier work by McCoy and Sibert,[17] is based on visualizing the quantum states in the classical angle space. For a specific eigenstate $|\Psi_\alpha\rangle$ of eq 1, with eigenenergy E_α, the semiclassical angle-space representation is obtained as

$$\Psi_\alpha(\boldsymbol{\psi}) \equiv \langle \boldsymbol{\psi} | \Psi_\alpha \rangle = \sum_{v \in \text{polyad}} C_{\alpha;\mathbf{v}} \exp(i\mathbf{v} \cdot \boldsymbol{\psi}) \qquad (5)$$

In the above equation, $C_{\alpha;\mathbf{v}}$ represents the contribution of the zeroth-order state $|\mathbf{v}\rangle$ (eigenstates of H_0 in eq 1) to the eigenstate and the restriction on the sum comes from the conserved polyads $\mathbf{K}$. As noted by Jung and Taylor, the semiclassical representation in eq 5 corresponds to the Fourier decomposition of Ψ_α onto the configuration space, N dimensional torus, of angles $\boldsymbol{\psi} \equiv (\psi_1, \cdots, \psi_N)$. One then analyzes the density and phase of $\Psi_\alpha(\boldsymbol{\psi})$ to provide a dynamical assignment. The crucial point here is that dynamical assignment is possible if the density is localized about one or more angle variables. Such localizations signal the importance of a specific number of independent resonances. Stated differently, the importance of a relatively small number of resonances is equivalent to the notion of dynamical decoupling mentioned earlier. For instance, the approximate decoupling $K_j \approx \tilde{K}_1 + \tilde{K}_2 + \tilde{K}_3$ implies that three independent resonances organize the eigenstates. Consequently, the density $|\Psi_\alpha(\boldsymbol{\psi})|^2$ is further reduced in dimensionality and becomes a function of $(N-3)$ angle (in general different from $\boldsymbol{\psi}$) variables. This $(N-3)$-dimensional angle space is now the organizing structure with three transverse directions along which the eigenstate exhibits localization. The relevant quantum numbers are then found by node counting of $|\Psi_\alpha(\boldsymbol{\psi})|^2$ along the transverse directions and phase advance (modulo 2π) around independent loops on the organizing structure.

In general, however, for $N \geq 3$ identifying the organizing structure requires dynamical guidance. This is not surprising in light of the aforementioned fact that the localizations are inherently dynamical in nature. At the same time, precisely due to the dynamical origins, obtaining the ideal organizing structure is a nontrivial task. For example, in the case of systems with $N = 3$ the configuration angle space is a three-dimensional torus. Visualizing the density and phase variations of $\Psi_\alpha(\boldsymbol{\psi})$ over such a three-dimensional torus might not be easy and one invariably has to resort to cuts through the space. Another complication comes from the fact that in a given energy range there might be several choices for the organizing structure. Again, dynamical considerations are essential to choose one organizing structure over the other. These points, and possible approaches to circumvent the problem, have been discussed in detail by Jung et al. in their recent analysis of the effective Hamiltonian for molecules like CDBrClF,[7] CF_3 CHFI,[8] and $SCCl_2$[9] with $N = 3$. Nevertheless, it is clear that uncovering the nature of the organizing structure through several appropriately chosen two-dimensional cuts becomes unwieldy with increasing N. We refer the reader to a recent comprehensive review[10] by Jung and Taylor for details.

3. Present Approach

3.1. Parametric Variations and "Level-Velocities". Note that the approach of Jung et al. does not explicitly require determining the periodic orbits and their bifurcations to dynamically assign the quantum states. In this sense it is an important step forward and a strong point in favor of their approach, but the need for visualizing the states restricts its utility. We remark here that similar concerns are responsible for abandoning techniques based on lifting the quantum states onto the appropriate Poincaré surface of sections.[50] Therefore, methods which do not require visualization are needed. One such method has been proposed by us earlier[13] and is based on studying the eigenstate expectation value of the resonance operators. Applications to several molecules like DCO, CHBrClF, and C_2H_2 with $N = 2$ has shown that it is possible to dynamically assign the quantum states. The assignments more or less agreed with those proposed using the method of Jung et al. and hence identifies the correct dynamical information encoded in the states.

The central object in our method is the expectation value (diagonal matrix element of an operator in the eigenbasis):

$$V_k^\alpha \equiv \langle \Psi_\alpha | \hat{V}_k | \Psi_\alpha \rangle = \frac{\partial E_\alpha}{\partial \tau_k} \qquad (6)$$

where the second equality follows from the Hellman−Feynman theorem.[51] The derivatives of the eigenvalues with respect to the resonant perturbation of interest are also known as "level-velocities" in the literature.[52,53,13] At the outset we mention that the expectation value and level-velocity are related to one another via eq 6. In particular, the qualitative insights provided by both the quantities are identical. However, quantitatively they can differ by a constant numerical factor which, for the

Hamiltonian of interest in eq 15, is easily determined. In subsequent discussions the terms expectation values and level-velocities will be used interchangeably. Several workers have established[54] the deep insights afforded by the level-velocities in studies involving quantum chaotic systems. It is also of relevance to note that the diagonal matrix elements play a central role in formulating a criterion for quantum ergodicity via the so-called Shnirelman−Colin de Verdiere-Zelditch (SCdVZ) theorem.[55] According to SCdVZ, in the semiclassical limit, the quantum eigenstate expectation values of certain operators is almost always the ergodic, microcanonical average of the classical phase space symbols corresponding to the operators. Thus, for an ergodic state

$$V_k^{\alpha} \approx V_k^{\mathrm{cl}} = \frac{2\int V_k(\mathbf{J},\boldsymbol{\psi})\delta[E_{\alpha} - H(\mathbf{J},\boldsymbol{\psi})]\,\mathrm{d}\mathbf{J}\mathrm{d}\boldsymbol{\psi}}{\int \delta[E_{\alpha} - H(\mathbf{J},\boldsymbol{\psi})]\,\mathrm{d}\mathbf{J}\mathrm{d}\boldsymbol{\psi}} \qquad (7)$$

for any choice of $\hat{V}_k$ and, conversely, violation of eq 7 implies the existence of localized states. Note that the resonant operators in eq 1 have a smooth classical limit $\hat{V}_k \rightarrow 2V_k$ $(\mathbf{J}, \boldsymbol{\psi})$. Subsequently, several studies[56−62] explored various aspects of SCdVZ, leading to important insights into the issue of quantum ergodicity. Detailed discussions, for example, can be found in the paper by Kaplan and Heller[56] and in the recent work[57] of Bäck et al. with several examples. Although in this work we do not specifically address the validity of the SCdVZ, it is clear that the notion of quantum ergodicity is intimately tied to the dynamical (un)assignability of the quantum states.

Semiclassical arguments for the connection between phase space objects causing localization and the quantum expectation values V_k^{α} has been given in many different contexts.[13,59−62,64] In essence the semiclassical considerations are based on analyzing the weighted spectral function $\sum_{\alpha} V_k^{\alpha}\delta(E - E_{\alpha})$ written in terms of periodic orbit sums. Mehlig et al.[61] have noted that the fluctuations of V_k^{α}, assuming $\hat{V}_k$ has a smooth classical limit and $[\hat{V}_k,\hat{H}] \neq 0$, reflect the inhomogeneities in the classical phase space and hence nonuniversal. Specifically, in the semiclassical limit

$$V_k{}^{\alpha} \approx \left(\frac{\rho_{\mathrm{c}}}{\rho_{\mathrm{tot}}}\right)V_{k;c}^{\alpha} + \left(\frac{\rho_{\mathrm{r}}}{\rho_{\mathrm{tot}}}\right)V_{k;r}^{\alpha} \qquad (8)$$

with ρ_{tot}, ρ_{r}, and ρ_{c} being the total, regular, and chaotic state densities, respectively. The chaotic and regular contributions to the expectation value are denoted by $V_{k;\mathrm{c}}^{\alpha}$ and $V_{k;\mathrm{r}}^{\alpha}$, respectively, with explicit semiclassical expressions based on the corresponding classical invariant structures. It has been argued that $V_{k;\mathrm{r}}^{\alpha}$ has as many limiting values as there are regular components in the phase space. The regular components (islands) are associated with periodic orbits.

Although the work by Mehlig et al.[61] and Boosé and Main[62] addresses the scaling system corresponding to a hydrogen atom in a strong magnetic field, recent independent work in the molecular context[13] shows that the expectation values can detect bifurcations and identify the birth of new modes in the nonscaling cases as well. For example, the occurrence of modes like the counter-rotator and local bender in C_2H_2[63] can be detected by the level velocities.[13] Importantly, from a computational perspective, the level velocities can be computed very easily by performing two diagonalizations. At the same time note that irrespective of the dimensionality of the system it is possible to identify the localized eigenstates by inspecting the two-dimensional plot of eigenvalue variations with changing the parameter of interest. Thus large $|V_k^{\alpha}|$, i.e., large level velocities, imply that the eigenstate $|\Psi_{\alpha}\rangle$ is localized in a regular part of the phase space characterized by the resonance $\mathbf{m}_k \cdot \boldsymbol{\Omega} \approx 0$.

3.2. "Lifting" the Eigenstates onto the Resonance Web: Time−Frequency Analysis. As discussed above, dimensionality constraints for systems with $N \geq 3$ lead to difficulties associated with techniques based on correlating the Husimi[65] or Wigner[66] functions of the eigenstates with the underlying phase space structures. On the other hand, several studies[67,69−71] on IVR from a time-dependent perspective have established the importance of the resonance or Arnol'd web, i.e., the various resonances and their disposition in the phase space. In other words, the key information is hidden in the various frequency lockings that an initial bright state experiences as a function of time. At the same time one can also obtain valuable information regarding the local structures in the phase space that influence the dynamics. Given the intimate connection between time and frequency domain descriptions of IVR, it is natural to expect the resonance web to play a crucial role in determining the nature of the eigenstates as well. However, to the best of our knowledge, an explicit connection between the resonance web and the quantum eigenstates has not been established to date. In this section we establish one such connection based on time−frequency analysis and hence "lift" the eigenstates onto the resonance web. The following sections provide concrete examples demonstrating the utility of the technique in conjunction with the level-velocity analysis.

Consider the reduced classical Hamiltonian (equivalent to considering the full D-dimensional Hamiltonian due to canonical invariance) of eq 4 and note that the lth time-dependent nonlinear frequency is given by

$$\dot{\psi}_l = \frac{\partial H(\mathbf{J},\boldsymbol{\psi})}{\partial J_l} = \frac{\partial H_0(\mathbf{J})}{\partial J_l} + 2\sum_k \tau_k \frac{\partial f_k(\mathbf{J})}{\partial J_l}\cos(\mathbf{m}_k \cdot \boldsymbol{\psi}) \equiv \Omega_l^0(\mathbf{J}) + \tilde{\Omega}_l(\mathbf{J},\boldsymbol{\psi}) \qquad (9)$$

wherein the zeroth-order frequency, time independent in the absence of the resonant perturbations, is denoted by $\Omega_l^0(\mathbf{J})$. The oscillatory part $\tilde{\Omega}_l(\mathbf{J}, \boldsymbol{\psi})$ becomes important if the system enters a resonant region. In general, presence of several independent resonances renders the system nonintegrable with the classical phase space being mixed regular−chaotic. Consequently, the nonlinear frequencies depend on time and exhibit large variations. However, several works[67−79] starting with the pioneering paper by Martens, Davis, and Ezra[67] have shown that even chaotic trajectories can exhibit regular behavior over large intervals of time. The main reason for such windows of regularity has to do with the inherently "sticky" nature of the Hamiltonian systems;[79] thus, a chaotic trajectory in the vicinity of a regular region in the phase space will "shadow" the local regular dynamics. In turn, the stickiness, lasting from a few to several picoseconds, leads to long time correlations and can have significant impact on the IVR dynamics.[67−73] Such windows of regularity, implicating specific resonances, can be identified by keeping track of the time-dependent nonlinear frequencies and appropriate ratios thereof.

Several methods[67−77] have been proposed to obtain the time-dependent frequencies, and in this work we follow the approach based on wavelet analysis.[75] Classical trajectories are computed over a time interval $[0, T]$ starting with the initial conditions $(\mathbf{J}(0), \boldsymbol{\psi}(0))$ chosen corresponding to specific values of the energy (e.g., eigenstate) and any other constants of the motion (polyads). The dynamical function $z_l(t) = (2J_l(t))^{1/2}\exp(i\psi_l)$ associated with the action-angle variables (J_l, ψ_l) for the lth-mode is then subjected to a wavelet transform[75]

$$L_g z_l(a,b) = a^{-1/2}\int_{-\infty}^{\infty} z_l(t) g^*\left(\frac{t-b}{a}\right) \mathrm{d}t \tag{10}$$

with $a > 0$ and real b. As in the previous studies we choose the Morlet−Grossman form for the mother wavelet

$$g(t) = \frac{1}{\sqrt{2\pi\sigma^2}} \exp\left(2\pi i\lambda t - \frac{t^2}{2\sigma^2}\right) \tag{11}$$

with $\lambda = 1$ and $\sigma = 2$. The wavelet transform in eq 10 yields the frequency content of $z_l(t)$ over a time window around $t = b$. In principle it is possible[76] to analyze all the frequencies, but for the purposes of this work it is sufficient to retain the dominant local frequency, i.e., $\Omega_l(t = b) = \max_a |L_g z_l(a,b)|$.

A general condition for resonant locking (commensurable frequencies) can be written down as

$$\alpha_1\Omega_1 + \alpha_2\Omega_2 + \ldots + \alpha_r\Omega_r = 0 \tag{12}$$

with integers $(\alpha_1, \alpha_2, \cdots, \alpha_r)$ and $\sum_k \alpha_k$ being the order of the resonance. The set of all resonances, at given $(E, \mathbf{K})$, up to some maximal order forms the resonance (Arnol'd) web to that order. Theoretically, with the knowledge of the zeroth-order Hamiltonian it is possible to determine the web explicitly via the intersection of the various resonance hyperplanes $\mathbf{m}_k \cdot \boldsymbol{\Omega}^0(\mathbf{J}) = 0$ with the relevant energy shell $H_0(\mathbf{J}) \approx E$. However, such a "static" construction cannot a priori highlight the dynamically significant regions of the resonance web except in the limit of small perturbations.[77] We, therefore, construct the "dynamical" web by the following procedure. Several trajectories with given $(E, \mathbf{K})$ are propagated and followed in the space of appropriately chosen, independent frequency ratios. Depending on the number of degrees of freedom, one can have several such spaces. For each trajectory the total number of visits to a given region of the frequency ratio space is recorded. The density plot, created by averaging and normalizing the number of visits over all the trajectories yields the resonance web.

Once the resonance web has been constructed as above, it is possible to identify the various resonance zones that are dynamically important at specific $(E, \mathbf{K})$. Note that, in general, $(\alpha_1, \alpha_2, \cdots, \alpha_r)$ might not belong to the set of primary resonances $\{m_k\}$. In such instances the observed locking in eq 12 can be shown to be induced by the primary resonances. If such induced lockings persist over long time scales, then they will manifest prominently in the resonance web and potentially influence the nature of certain quantum eigenstates. Clearly, if one can lift the quantum states onto the resonance web, then the dominant influences can be ascertained immediately. But how does one lift the quantum states onto the resonance web? We now propose a method based on the time-frequency analysis discussed above. In essence, our method provides a higher dimensional analog to the two degrees of freedom procedure involving superposing the Wigner or Husimi function of a state onto the Poincaré surface of section.

We begin by noting that a specific eigenstate $|\alpha\rangle$ with eigenvalue E_α can be expressed as a linear combination of the zeroth-order number states $|v\rangle$ (with energy $E_{\mathbf{v}}^0$) as

$$|\alpha\rangle = \sum_{\mathbf{v}} C_{\mathbf{v}}^{\alpha} |\mathbf{v}\rangle \tag{13}$$

The quantity, $|C_{\mathbf{v}}^{\alpha}|^2$ is the relative contribution of the zeroth-order state $|\mathbf{v}\rangle$ to $|\alpha\rangle$. Semiclassically, one associates classical zeroth-order actions (well-defined since $H_0(\mathbf{J})$ is integrable) $\mathbf{J}$ with every zeroth-order quantum state $|\mathbf{v}\rangle$ via the rule

$$v_l \leftrightarrow \left(J_l + \frac{d_l}{2}\right)\hbar \tag{14}$$

with d_l being the degeneracy of the lth mode. Therefore, for a specific $|\mathbf{v}\rangle$ in the expansion eq 13 we fix the classical actions according to eq 14 and generate several initial conditions $(\mathbf{J}_v(0), \boldsymbol{\psi}(0))$ such that $H(\mathbf{J}_v, \boldsymbol{\psi}) = E_{\mathbf{v}}^0$. The classical dynamics ensuing from each initial condition is subjected to the wavelet transform and followed in the frequency space as before. The number of visits to a particular region in the frequency ratio space is averaged over the initial angles weighted by $|C_{\mathbf{v}}^{\alpha}|^2$. This is crucial since $|C_{\mathbf{v}}^{\alpha}|^2$ properly takes into account the relative contribution by the specific zeroth-order state. The procedure is repeated for every one of the zeroth-order states contributing in eq 13, and the weighted densities at each cell of the space, arising from every $|\mathbf{v}\rangle$, are added together. Finally, the densities are normalized to one and the resulting lifted eigenstate is compared to the $(E_\alpha, \mathbf{K})$ resonance web.

A few comments are in order at this stage. First, for localized eigenstates we expect there to be considerable difference between the resonance web and the lifted eigenstate. On the other hand, lifts of delocalized eigenstates in any independent frequency ratio space should show the same overall features as that of the resonance web, in accordance with the SCdVZ theorem. Second, there might arise questions regarding the basis-set dependence of the lift. Expressing $|\alpha\rangle$ in a different basis would entail the usage of a different set of zeroth-order classical actions. However, the invariance of classical dynamics under canonical transformations (corresponding to the unitary basis change) ensures that the observed features are left invariant. Third, from the perspective of computational ease, it is useful to impose a cutoff $|C_{\mathbf{v}}^{\alpha}|^2 \leq \epsilon$ in order to restrict the total number of zeroth-order states that need to be considered for the lifting procedure. Note that convergence can be easily checked by varying ϵ, and in this work we set it to a value of 0.005.

4. Application

4.1. Spectroscopic Hamiltonian. The effective Hamiltonians of interest in this work pertain to the high-frequency modes of the two molecules CDBrClF and CF_3 CHFI. The fitted Hamiltonian for CDBrClF has been determined by Beil et al.[29] based on experimental spectra covering all the fundamentals and CD-stretching overtones up to polyad $N = 5$ of CDBrClF. The four high-frequency normal modes of CDBrClF correspond to CD stretch (ν_s), CF stretch (ν_f), and the two CD bends (ν_a and ν_b). Beil et al. noted in their work that restricting their fit to the three CD normal modes does not even approximately account for the observed spectra, and hence the CF stretching mode has to be included. In a companion paper, Pochert et al. fitted the CF_3 CHFI spectrum[30] in a similar fashion with CH stretch (ν_s), CF stretch (ν_f) and the two CH bending modes (ν_a and ν_b). Since both the effective Hamiltonians have identical structure, we analyze them together in this work.

The effective Hamiltonian $H = H_0 + V_{\mathrm{res}}$ with the anharmonic zeroth-order part

$$H_0 = \sum_j \omega_j a_j^\dagger a_j + \sum_{i\leq j} x_{ij} a_i^\dagger a_i a_j^\dagger a_j \tag{15}$$

has a total of nine resonant perturbations included in V_{res}. These anharmonic resonances representing the off-diagonal coupling between the four modes are

$$V_{\mathrm{res}} = \sum_{j\le m}^{a,b,f} \frac{k_{sjm}}{2\sqrt{2}}(a_s a_j^\dagger a_m^\dagger + a_s^\dagger a_j a_m) + \frac{1}{2}\sum_{j<m}^{a,b,f} \gamma_{jm}(a_j^\dagger a_j^\dagger a_m a_m + a_j a_j a_m^\dagger a_m^\dagger) \quad (16)$$

The harmonic creation and destruction operators for the jth mode are denoted by $a_j^\dagger$ and a_j, respectively. Note that despite the four coupled modes the system has effectively three degrees of freedom due to the existence of a conserved polyad

$$N = v_s + \frac{1}{2}(v_f + v_a + v_b) \quad (17)$$

and the number of states, for integer N given by

$$W_N = \frac{1}{2}\left\{\frac{1}{3}(N+1)[4(N+1)^2 - 1] + (N+1)^2\right\} \quad (18)$$

We restrict ourselves to the $N = 5$ (total of 161 eigenstates) polyad for both molecules. The Hamiltonian parameter values are taken from the fit provided in the experimental works[29,30] and are reproduced in Table 1 for convenience. It is important to note that for both molecules the Fermi resonance strengths k_{sjm} are quite large; in fact the strengths are larger than the mean energy level spacings of H_0 for polyad $N = 5$. On the other hand, the Darling−Dennison strengths γ_{jk} are considerably larger in the case of CF_3 CHFI as compared to those of CDBrClF. The presence of several strong anharmonic resonances implies that one should expect extensively mixed eigenstates for both the systems.

4.2. Classical Limit Hamiltonian. The classical limit of the above effective Hamiltonian, after proper symmetrization,[7] is obtained in the usual fashion by invoking the Heisenberg correspondence[49]

$$a_j \rightarrow \sqrt{I_j}e^{-i\phi_j}, \qquad a_j^\dagger \rightarrow \sqrt{I_j}e^{i\phi_j} \quad (19)$$

with $(\mathbf{I}, \boldsymbol{\phi})$ being the unperturbed action-angle variables. In terms of $(\mathbf{I}, \boldsymbol{\phi})$ the classical Hamiltonian takes the form

TABLE 1: Spectroscopic Hamiltonian Parameters (in cm^{-1})

parameter	CDBrClF[a]	CF_3CHFI[b]
ω_s	2285.80	3026.60
ω_f	1088.22	1306.60
ω_a	974.22	1369.50
ω_b	919.20	1240.60
x_{ss}	−34.30	−53.60
x_{ff}	−6.99	−6.50
x_{aa}	−1.91	−4.40
x_{bb}	−1.24	−5.40
x_{sf}	−5.59	−4.90
x_{sa}	−17.33	−12.70
x_{sb}	−17.24	−17.70
x_{fa}	−5.16	−14.10
x_{fb}	0.18	−1.40
x_{ab}	1.40	−3.20
k_{sff}	50.70	41.10
k_{saa}	39.50	65.80
k_{sbb}	59.80	55.30
k_{sfa}	98.00	61.80
k_{sfb}	−91.30	20.70
k_{sab}	91.80	17.50
γ_{ab}	−1.10	−21.10
γ_{fa}	−1.70	−15.30
γ_{fb}	4.00	−26.70

[a] Values from Table 8 in ref 29 (last column $H^{4D}_{\mathrm{eff,MP2}}$). [b] Values from Table 1 in 30 (sixth column $H^{4D}_{\mathrm{sc\text{-}IP}}$).

$$H(\mathbf{I}, \boldsymbol{\phi}) = H_0(\mathbf{I}) + V_{\mathrm{res}}(\mathbf{I}, \boldsymbol{\phi}) \quad (20)$$

with

$$H_0(\mathbf{I}) = \sum_j \tilde{\omega}_j I_j + \sum_{i\le j} x_{ij} I_i I_j - E_0 \quad (21)$$

being the zeroth-order integrable part and E_0 is the zero-point energy. In the above, the new frequencies $\tilde{\boldsymbol{\omega}}$ are determined in terms of the old frequencies $\boldsymbol{\omega}$ and anharmonicities $\{x_{ij}\}$. The resonant perturbations similarly can be expressed as:

$$V_{\mathrm{res}}(\mathbf{I}, \boldsymbol{\phi}) = \sum_{j\le m}^{a,b,f} \frac{k_{sjm}}{\sqrt{2}}\sqrt{I_s I_j I_m}\cos(\phi_s - \phi_j - \phi_m) + \sum_{j<m}^{a,b,f} \gamma_{jm} I_j I_m \cos(2\phi_j - 2\phi_m) \quad (22)$$

As in the quantum case the classical Hamiltonian also has effectively three degrees of freedom due to the exact conservation of the classical polyad $K = I_s + (I_f + I_a + I_b)/2 = P + 5/4$.

Explicit dimensional reduction to three degrees of freedom can now be performed by recognizing the existence of K, i.e., by doing an appropriate canonical transformation:[7]

$$F = \frac{1}{2}\sum_k^{a,b,f} J_k(2\phi_k - \phi_s) + K\phi_s \quad (23)$$

resulting in the new Hamiltonian

$$H(\mathbf{J}, \boldsymbol{\psi}; K) = \sum_j^{a,b,f} \bar{\omega}_j J_j + \sum_{j\le k}^{a,b,f} \bar{x}_{jk} J_j J_k + \Delta + \frac{1}{\sqrt{2}}\sum_{j\le k}^{a,b,f} k_{sjm}\sqrt{I_s J_j J_k}\cos(\psi_j + \psi_k) + \sum_{j\ne k}^{a,b,f} \gamma_{jk} J_j J_k \cos(2\psi_j - 2\psi_k) \quad (24)$$

depending only on the angles $\psi_k = (2\phi_k - \phi_s)/2$ and their conjugate actions $J_k = I_k$ with $k = a, b, f$. The parameters $\bar{\boldsymbol{\omega}}$, $\bar{\mathbf{x}}$, and Δ can be expressed in terms of the original parameters.

5. Analysis of the Eigenstates

In the present situation the approach based on level velocities is challenging since there are nine perturbing resonances. Due to the presence of several strong Fermi resonances (50−100 cm^{-1}) one expects strongly mixed eigenstates. Nevertheless, we show below that the level velocities can identify the localized states interspersed among the highly mixed states. However, we start our analysis by looking at another useful, albeit basis-dependent, measure known as the inverse participation ratio (IPR). The IPR provides information on the extent of mixing of the eigenstates and has been extensively utilized in earlier studies. We make a few pertinent observations, based on computing the IPR of the eigenstates in various basis, which later aid in the analysis of the level velocities.

5.1. Inverse Participation Ratios. The IPR associated with an eigenstate $|\alpha\rangle$ in a specific basis $\{|\mathbf{l}\rangle\}$ is computed as

$$L = \sum_{\mathbf{l}} |\langle \mathbf{l}|\alpha\rangle|^4 \quad (25)$$

In the present case there are several choices for the basis. We report here the IPR in the zeroth-order $|\mathbf{n}\rangle$ basis L_0 and the IPRs in basis with a specific mode j decoupled from the rest L_{-j}. For example, the L_{-s} denotes computations in a basis in which the mode s is decoupled from the modes f, a, and b. In other words

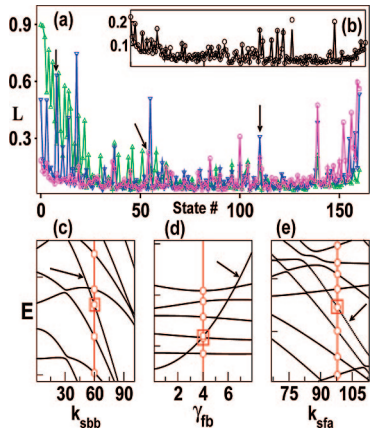

Figure 1. Inverse participation ratios for CDBrClF eigenstates belonging to polyad $N = 5$. (a) The IPRs L_{-j} in the jth mode decoupled basis (cf. eq 26) are shown with $j = f$ (green triangles), $j = a$ (blue triangles), and $j = b$ (magenta circles). The inset (b) shows L_{-s} (circles) and the zeroth-order basis (line) IPR L_0. Panels c, d, and e show select eigenstates (indicated by arrows in (a) corresponding to states 9, 111, and 55, respectively) exhibiting linear parametric motion with respect to specific resonances. The vertical line (red) corresponds to the actual resonance strength. Only the first two states are dynamically assignable. In the bottom panels the energy range is about 50 cm^{-1} centered about the specific eigenstates of interest. See text for explanations.

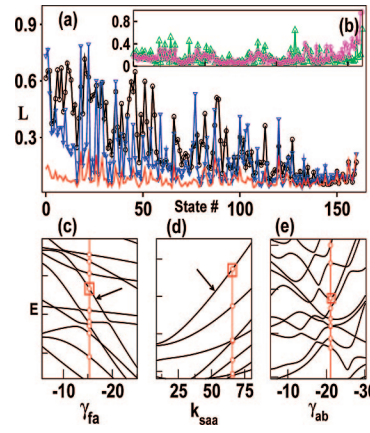

Figure 2. Same as in Figure 1 for CF_3CHFI eigenstates belonging to polyad $N = 5$. (a) IPRs L_{-s} (black circles), L_{-a} (blue triangle down), and L_0 (red) are shown. Inset (b) L_{-f} (green triangles) and L_{-b} (magenta circles). Note the difference in the y-axis scale between Figure 1b and Figure 2b. Panels c, d, and e show level velocities of states 20, 161, and 80, respectively, with respect to specific resonances. The first two states, exhibiting linear parametric motion, are localized and hence dynamically assignable. The last state is an example of a mixed state.

the basis used in the computation of L_{-s} are eigenstates of the three-mode subsystem

$$H_{-s} = H_0 + \sum_{j<m}^{a,b,f} \gamma_{jm}(a_j^\dagger a_j^\dagger a_m a_m + \text{h . c . })/2 \qquad (26)$$

Therefore, a high value of L_{-j} implies a strong decoupling of the jth mode. However, as a cautionary note we remark that such an interpretation holds true as long as no new modes have been created as a result of classical bifurcations.[13] Note that decoupling two of the modes, say j and k, to obtain L_{-jk} in the present case of interest is the same as computing the IPRs in various single resonance basis.

In parts a and b of Figure 1 we show the relevant IPRs. We mention here that single resonance basis IPRs (not shown), apart from very few states, are comparable to L_0 implying the influence of multiple resonances on a large fraction of the eigenstates. From Figure 1b it is clear that over the entire energy range the s mode is strongly coupled. This is due to the fact that both the L_0 and L_{-s} have nearly the same small values. At the same time the result for L_{-f}, shown in Figure 1a, suggests that the f mode is decoupled at lower energies. Specifically, starting from the bottom of the polyad up to an energy of about 9600 cm^{-1} the eigenstates show very large values for L_{-f} and hence the unimportance of the f mode. In the same energy region we observe that the b mode is strongly coupled whereas for certain states the a mode seems to be decoupled. These observations contradict the earlier work[7] wherein it is claimed that the first 64 states could be assigned based on the $\Omega_a \approx \Omega_b$ alone, i.e., decoupling of the modes s and f over the energy range 8908−9817 cm^{-1}. However, the IPR analysis suggests that it is more reasonable to assume that the f mode is decoupled up to about 9500 cm^{-1}.

In a similar fashion panels a and b of Figure 2 show the IPR data for CF_3CHFI eigenstates. It is clear that the s and a modes are decoupled over a fairly large energy range starting from the bottom of the polyad. Consistently, Figure 2b indicates the strong coupling of the f and b modes and these observations are in accordance with the earlier study[8] wherein a large number of states were seen to be organized by the $\Omega_f \approx \Omega_b$ resonance. However, there are exceptions that can be seen in Figure 2b involving a few states with rather large values of L_{-f}. Thus, the analysis of IPR and their differences, as evident from comparing Figures 1 and 2, immediately yields two important pieces of information that can aid in the dynamical assignment of the states. First, the fraction of states exhibiting strong mixing of all four modes is considerably more in the case of CDBrClF as seen in Figure 1a,b in the middle of the polyad. Second, the complicated interleaving of high and low values of IPRs in both systems reflects the interleaved sequences of states uncovered by Jung et al. in their work.[7,8]

The IPR analysis cannot give any more information regarding the dynamical assignment. In particular there is no possibility of extracting a set of approximate quantum numbers from the IPR data alone. Therefore we now analyze the states using the methods described in section 3 for a more detailed understanding. However, instead of providing an exhaustive list of dynamical assignments for every state in the polyad, as has been done[7,8] by Jung et al., from here on we focus on a few representative examples in order to illustrate our approach and contrast with the earlier work. Nearly all of the states can be classified as belonging to the three classes represented by the selected examples. In the case of CDBrClF we take states 9, 55, and 111 as examples and in the case of CF_3CHFI the exemplary states are 20, 80, and 161. The first state of both systems (9 and 20) are examples of states whose previous assignment is not supported by our analysis. The second set of states (111 and 161) are examples for which our assignment agrees with those provided earlier. On the other hand, the states 55 and 80 are examples of states that pose a considerable challenge for the dynamical assignment. The relevant IPR and level-velocity information are shown in Table 2 and Table 3, respectively. In what follows, we show that IPR and level-velocity information combined with the state space and phase space representations yield detailed insights into our ability or inability to dynamically assign the selected states.

5.2. Level Velocities. In light of the IPR analysis indicating the decoupling of certain modes, we now ask the following question: Can the level velocities identify the corresponding localized states? Inspired by the SCdVZ theorem, it is possible

TABLE 2: IPR in Various Basis for the Example States Discussed in the Paper[a]

	state	E_α	L_0[b]	L_{-s}	L_{-f}	L_{-a}	L_{-b}	L_{-jk}[d]
CDBrClF	9	9278	0.16	0.14	0.27	**0.63**[c]	0.11	0.25 (*sbb*)
	55	9749	0.04	0.06	0.04	0.04	**0.23**	*
	111	10164	0.19	0.25	0.19	**0.35**	0.22	0.25 (*fb*)
CF_3CHFI	20	12283	0.08	**0.43**	0.07	0.15	0.30	0.17 (*fa*)
	80	13016	0.04	**0.15**	0.05	0.08	0.06	*
	161	14173	0.22	0.17	0.66	0.21	**0.97**	0.64 (*saa*)

[a] Cf. eq 26. [b] IPR in the zeroth-order basis. [c] The highest IPR value, indicating specific weakly coupled mode(s), are shown in bold. [d] Largest IPR in a single resonance basis (indicated within brackets) and * indicates the absence of any dominant value.

to identify the existence of localized states since, for a delocalized state one expects eq 7 to hold for any perturbing operator. Violations of eq 7 signal the existence of localized states, and based on the earlier work of Peres and co-workers the localized states are expected to show regular patterns in the plots of V_k^α versus E_α. In addition it is possible to provide classical estimates for the expectation values when $|\alpha\rangle$ localizes about (un)stable periodic orbits corresponding to specific resonances.[13] For example, the classical maximal level-velocity estimate for a state localized about the fixed point (periodic orbit) corresponding to the $\Omega_s \approx 2\Omega_b$ Fermi resonance is

$$\left(\frac{\partial E_\alpha}{\partial k_{sbb}}\right)_{\mathrm{cl}} = \pm\left(\frac{2P_{sbb}}{3}\right)^{3/2} \tag{27}$$

with $P_{sbb} \equiv v_s + v_b/2$ being the subpolyad and the $\pm$ sign being associated with the values $\psi_b = 0, \pi/2$ of the resonant angle at the fixed point. Similarly

$$\left(\frac{\partial E_\alpha}{\partial \gamma_{ab}}\right)_{\mathrm{cl}} = \pm P_{\mathrm{ab}}^2 \tag{28}$$

is the classical estimate for the maximum level-velocity of a state localized in the $2\Omega_a \approx 2\Omega_b$ Darling−Dennison resonance zone with the appropriate subpolyad $P_{ab} \equiv (v_a + v_b)/2$ and fixed point angle $(\psi_a - \psi_b) = 0, \pi/2$. Analogous expressions can be written down for the rest of the resonance term in eq 15. It is, however, important to note that the classical estimate would be P_{ab} for states influenced by the $\Omega_a \approx \Omega_b$ resonance. Therefore, the level-velocity measure can distinguish between states that are influenced by the primary Darling−Dennison resonance and those influenced by an induced 1:1 resonance. The classical estimates allow one to pick the dominant resonance organizing a specific localized state in cases wherein large deviations from the SCdVZ are observed for more than one resonant perturbation.

In parts a and b of Figure 3 we show the expectation values V_{sbb}^α and V_{ab}^α, respectively, for the $N = 5$ polyad of CDBrClF. In both cases one can clearly observe several states violating eq 7 and hence localized. In particular, at the lower end of the polyad, shown in Figure 3c,d, it is possible to discern the regular patterns associated with the localized states. Note that the occurrence of regular patterns in Figure 3c,d is in agreement with the uncovering of regular sequence of states in the previous analysis of Jung et al. with the dynamical assignments $(l_f = v_f, l_{a+b} \equiv 2P_{ab}, t)$. Although we agree with the appearance of regular states at the lower end of the polyad, there is an important difference—the sequences are much more regular with respect to V_{sbb}^α as compared to V_{ab}^α. In particular, one of the sequences (corresponding to $(2, 8, t)$ and shown as a red line in Figure 3d) is significantly perturbed. The IPR data in Table 2 clearly indicates the decoupling of mode a since $L_{-a} \approx 0.63$. In addition, Table 3 shows that the expectation value V_{ab} is much smaller than the maximal classical estimate in eq 28 for a state with $P_{ab} = 4$. In the next section we show the state space and phase space representations for the first member of the sequence (state 9) to confirm the predictions.

In Figure 4 the three Darling−Dennison expectation values V_{fb}^α, V_{fa}^α, and V_{ab}^α are shown for the $N = 5$ eigenstates of CF_3CHFI. The choice of the operators, out of the possible nine in eq 15, is motivated by the previous assignment[8] of a large number of states with the $\Omega_f \approx \Omega_b$ locking. This is confirmed in Figure 4a which shows several states, some forming a regular pattern, exhibiting strong deviations from the classical ergodic value. However, as seen from parts b and c of Figure 4, there exist states which show significant deviations with respect to the $\Omega_f \approx \Omega_a$ and $\Omega_a \approx \Omega_b$ lockings as well. For example, the expectation values V_{ab}^α shown in Figure 4c indicate that several states lying in the energy region 13000−13600 cm^{-1} are strongly influenced by the $\Omega_a \approx \Omega_b$ Darling−Dennison resonance. Interestingly, previous work[8] precisely identifies the same energy region supporting a few of the "exceptional" states which show a simple phase structure of $\Psi_\alpha(\psi)$ only in the $\psi_a = \psi_b +$ const plane. It is worth pointing out that such information is obtained within our approach in a straightforward manner.

As another example of the power and utility of the level-velocities, in Figure 4a we show two of the eigenstate sequences uncovered by the previous authors.[8] The sequences correspond to states which are dynamically assigned as $(l_a, l_{b+f}, t) = (0, 10, t)_+$ (red line) and $(1, 9, t)_+$ (blue line) with varying values of the transverse quantum number t relative to the plane $\psi_f = \psi_b$. However, from the perspective of the level velocities, one of the states in the $(0, 10, t)_+$ sequence stands out in terms of the expected linearly decreasing trend. On closer inspection it is indeed found that the state in question is not organized by the $\Omega_f \approx \Omega_b$ lock. Instead, a different state fits the sequence and the resulting corrected sequence is shown in Figure 4a by dotted red line. Similarly, one of the states in the $(1, 9, t)_+$ sequence is much better described as a $\Omega_f \approx \Omega_a$ state since, as shown in Figure 4b (blue square) and Table 3, it exhibits a much larger V_{fa}^α as compared to V_{fb}^α. Further evidence for our assignment from both the state space and phase space perspective is provided in the following section.

Before ending this section we note that, given the scaling (cf. eqs 27 and 28) of the level velocities with the approximate subpolyads, inspecting Figures 3b and 4 one can infer that some of the lowest energy states of CDBrClF are influenced by the induced Ω_a:Ω_b = 1:1 resonance as opposed to the $2\Omega_a \approx 2\Omega_b$ Darling−Dennison resonance. Our dynamical calculations show that several of the two and three mode Fermi resonances are active over the entire energy range. In contrast, for CF_3CHFI we observe that the dynamics is dominated by the three Darling−Dennison resonances.

5.3. Quantum States in State Space and Phase Space. In this section we take the exemplary states mentioned in the previous section and lift them onto the classical phase space using the procedure given in section 3.2. In addition, select states are also represented in the discrete zeroth-order quantum number space (state space) with the analogous classical zeroth-order action space as a template. A prime motivation for showing the state space representation, apart from demonstrating the classical-quantum correspondence, comes from several studies which show that IVR is best understood as a diffusive process in the quantum state space.[80] The classical state space template provides information regarding the nature of the dynamics and is constructed as follows. Several initial $(\mathbf{J}, \boldsymbol{\psi})$ are chosen with

TABLE 3: Quantum Expectation Values versus Classical Ergodic Average for the Select States[a]

	state	V_{sff}	V_{saa}	V_{sbb}	V_{sfa}	V_{sfb}	V_{sab}	V_{ab}	V_{fa}	V_{fb}
CDBrClF	9	−0.86	−0.32	**−6.25** [b]	−0.13	2.69	−0.14	3.14	0.06	−2.78
		−0.39	−2.34	−2.67	−1.16	0.91	−2.54	0.37	1.17	−0.95
	55	−2.97	−1.71	0.05	**−3.50**	0.94	−0.99	1.26	0.18	0.03
		−1.09	−0.26	0.13	−1.34	0.52	−0.62	−0.70	−0.25	−0.73
	111	−2.57	0.01	−0.11	0.39	−0.82	0.21	0.10	0.22	**9.68**
		−0.39	0.82	0.95	0.18	−0.66	0.69	0.05	−0.61	0.67
CF_3CHFI	20	−0.94	−0.55	−1.10	0.26	−0.06	−0.02	2.20	**20.22**	1.18
		−1.16	−1.01	−1.50	−0.69	−0.41	−0.37	6.22	5.89	6.57
	80	0.55	−0.05	−0.43	−0.88	0.13	−0.19	−1.17	**−7.04**	−2.75
		0.04	−1.05	0.24	−0.74	−0.38	−0.34	−1.98	−2.55	−5.48
	161	0.38	**13.46**	−0.16	3.12	0.26	0.80	−0.39	0.87	−0.01
		1.41	11.43	−0.02	3.97	0.37	0.86	−1.01	−0.92	−0.08

[a] Classical values are shown below the corresponding quantum values and calculated using eq 7. [b] Quantum values deviating significantly from the classical ergodic values are shown in bold.

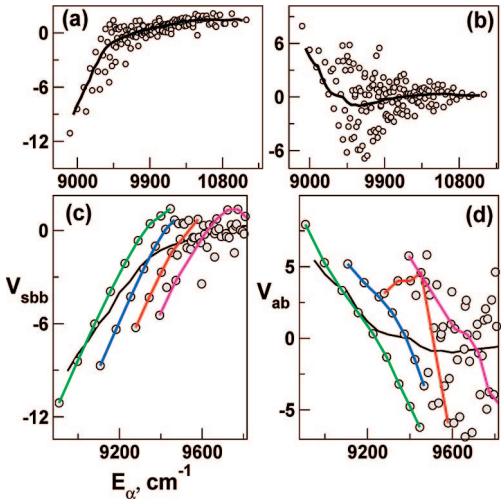

Figure 3. Quantum expectation values for the CDBrClF eigenstates with polyad $N = 5$. Panels a and b show V^{α}_{sbb} and V^{α}_{ab}, respectively. The quantum expectations are compared to the respective classical microcanonical averages V^{cl} calculated using eq 7 (solid line). Note the strong deviations of V^{α} from V^{cl} manifesting as regular patterns at lower energies. Parts c and d focus on the lower energy regions wherein some of the eigenstate sequences (color lines), predicted earlier, are also shown. Clearly, the sequences are better organized by the $\Omega_s \approx 2\Omega_b$ Fermi resonance.

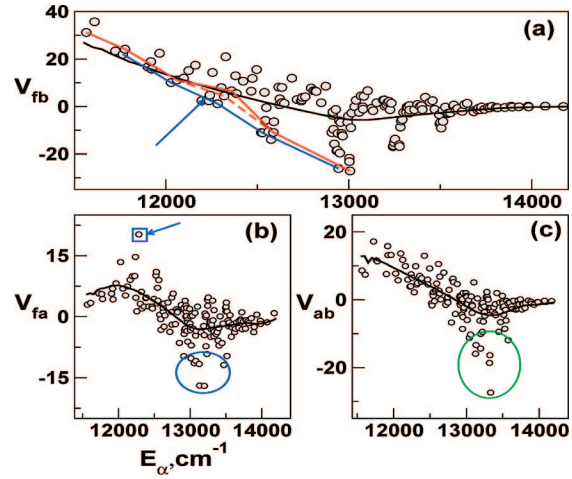

Figure 4. Same as in Figure 3 but for the $N = 5$ eigenstates of CF_3CHFI. Quantum expectation values of the three Darling−Dennison resonances are shown. In (a) two eigenstate sequences (red and blue) identified by Jung et al. are also shown. The corrected sequence $(0, 10, t)_+$ is shown as dotted red line. Panels b and c show regions (blue and green circles) wherein localized states are not organized by the $\Omega_f \approx \Omega_b$ resonance. In (a) one of the states (blue arrow) of the $(1, 9, t)_+$ sequence is influenced by $\Omega_f \approx \Omega_a$ resonance as evident from the large V^{α}_{fa} seen in (b). Some of these states have been labeled "exceptional" by the previous authors. See text for details.

the energy constraint $H(\mathbf{J}, \boldsymbol{\psi}; K) = E_\alpha$ and classical trajectories are propagated from $t = 0$ to some sufficiently large time $t = T$. The time-frequency analysis of the trajectories is used to define a diffusion constant associated with the kth-mode as

$$d_k(T) = \frac{1}{T}\int_0^T |\Omega_k(t) - \bar{\Omega}_k| \, dt \qquad (29)$$

with $\bar{\Omega}_k$ being the average frequency. From the definition of $d_k(T)$ given above, it follows that $d_k(T) \approx 0$ for regular dynamics and also for dynamics that exhibits significant stickiness around regular regions over the time interval of interest. However, chaotic dynamics leads to large frequency variations and hence lead to large, nonvanishing $d_k(T)$. The diffusion constant associated with all the modes can be determined and we associate $\Sigma_k d_k(T)$ with the specific point (I_s, I_f, I_a, I_b) in the state space.

5.3.1. Localized States. To start with, note that all three states of CDBrClF exhibit linear parametric motion with respect to specific resonances as shown in parts c, d, and e of Figure 1. Similar observations hold for the selected states of CF_3CHFI, with perhaps the exception of state 80, as seen in parts c, d, and e of Figure 2. At this stage it is worth emphasizing that such linear parametric motion of the eigenvalues with varying coupling strengths is indicative of localized states. Thus, referring to Table 3, the CDBrClF states 9 (9278 cm^{-1}) and 111 (10164 cm^{-1}) exhibit linear parametric motion with large $|V^{\alpha}_{sbb}|$ and $|V^{\alpha}_{fb}|$, respectively. Therefore, it is expected that state 9 is organized by the $\Omega_s \approx 2\Omega_b$ Fermi resonance whereas state 111, classified previously as an exceptional state in the dense region of the polyad, is under the influence of $\Omega_f \approx \Omega_b$ resonance. Along the same lines, linear parametric motion of the CF_3CHFI states 20 (12283 cm^{-1} with large $|V^{\alpha}_{fa}|$) and 161 (14172 cm^{-1} with large $|V^{\alpha}_{saa}|$) indicate (see Table 3) them to be localized in the $\Omega_f \approx \Omega_a$ and $\Omega_s \approx 2\Omega_a$ resonance zones, respectively.

Parts a and b of Figure 5 show the state space viewpoint of the regular states 9 and 20, respectively, along with the classical template. The dominant influence of $\Omega_s \approx 2\Omega_b$ resonance on state 9 is clearly evident from Figure 5a. Specifically, the state is localized along the $P_{sbb} \equiv n_s + n_b/2 = 4$ subpolyad characterized by the large diffusion region in the classical state space as well. These observations agree with the level-velocity predictions shown in Figure 3c and the IPR data in Table 2. Moreover, the (I_a, I_b) state space projection of state 9 (not shown

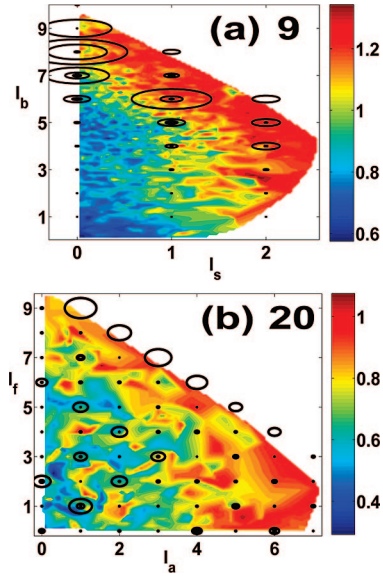

Figure 5. Quantum states 9 (a) and 20 (b) projected onto the (I_s, I_b) and (I_a, I_f) state spaces, respectively. The radius of the circle at each state space point $|v\rangle$ corresponds to the amplitude C_α^v. The angle-averaged classical diffusivities at each state space point forms the classical template. State 9 is delocalized along the polyad $P_{sbb} \equiv n_s + n_b/2 = 4$ and state 20 corresponds to $P_{fa} \equiv (n_f + n_a)/2 = 5$. Note that (a) and (b) are constructed using 2000 and 400 state space points, respectively. The diffusion data at each state space point is obtained by averaging over a set of 10 initial angle variables.

here) does not localize along $P_{ab} \equiv (n_a + n_b)/2 = 4$ as predicted earlier[7] which explains the perturbation in the level-velocity sequence seen in Figure 3d. Similarly, the state space projection of CF_3CHFI state 20 shown in Figure 5b establishes the dominance of $\Omega_f \approx \Omega_a$ resonance with localization along the subpolyad $P_{fa} \equiv (n_f + n_a)/2 = 5$. Notice the ease with which the same information is obtained by the level-velocity analysis summarized in Figure 4b. Although not shown here, the state spaces for states 111 and 161 show clean features and exhibit localization in the low diffusion regions.

In order to confirm the nature of the localized states as predicted by the level velocities, consistent with the IPR information, we lift the states onto the classical resonance web using the procedure described in section 3.2. The results for CDBrClF in terms of both the (E_α, N) web and the eigenstate-lifted web are shown in Figure 6. As expected from Figure 3b, and in contrast to the earlier work,[7] one can clearly see from Figure 6a that the state 9 is influenced strongly by the $\Omega_s \approx 2\Omega_b$ Fermi resonance. In particular we have confirmed that at lower energies the average locking time in the $\Omega_s \approx 2\Omega_b$ resonance is atleast a factor of 3 larger than that in the $\Omega_a \approx \Omega_b$ resonance. The results for state 111 shown in Figure 6c clearly identifies it as a $\Omega_f \approx \Omega_b$ state. The striking difference in the appearance of the (E_α, N) web and the lifted eigenstate shows the exceptional character of the state. More specifically this means that the dynamics of of the zeroth-order states which maximally contribute to the state 111 are dominated by the $\Omega_f \approx \Omega_b$ lock.

In Figure 7 the phase space representations of the CF_3CHFI eigenstates are shown. The case of state 20, discussed in the previous section, demonstrates the utility of the present approach. The striking shift of maximal density observed in Figure 7a from $\Omega_f \approx \Omega_b$ to $\Omega_f \approx \Omega_a$ region of the web confirms the level-velocity predictions of Figure 4b. Despite the $\Omega_f \approx \Omega_a \approx \Omega_b$ lock implied by the figure, the density shift indicates that state 20 is more appropriately classified as a $\Omega_f \approx \Omega_a$ state. Interestingly, as a further confirmation of our assignment we have checked that the angle space density $|\Psi_{20}(\psi)|^2$ (cf. eq 5) indeed exhibits localization along the diagonal in the $\psi_f = \psi_a$ plane. The other localized case of state 161 at the energetic top of the polyad is shown in Figure 7c. As is evident from the figure, the localization is mainly due to the $\Omega_s \approx 2\Omega_a$ Fermi resonance consistent with the IPR and level-velocity results of Figure 2. In this case our results concur with the earlier[8] assignment.

5.3.2. Mixed States. In contrast to the above-mentioned regular states, the CDBrClF state 55 (9749 cm^{-1}) and CF_3 CHFI state 80 (13016 cm^{-1}) are two examples of mixed states. The former state has not been assigned in the previous work[7] whereas the latter state has been termed[8] as an unusual state *involving locking of all modes without implying any pairwise locking*. These two states represent examples of two different ways in which highly mixed states can arise. State 55 is not involved in any avoided crossing and, despite exhibiting linear parametric motion (cf. Figure 1e) with respect to the multimode $\Omega_s - \Omega_f - \Omega_a \approx 0$, is not a pure multimode state. On the other hand, state 80 is involved in avoided crossing with multiple states and does not exhibit linear parametric motion with respect to

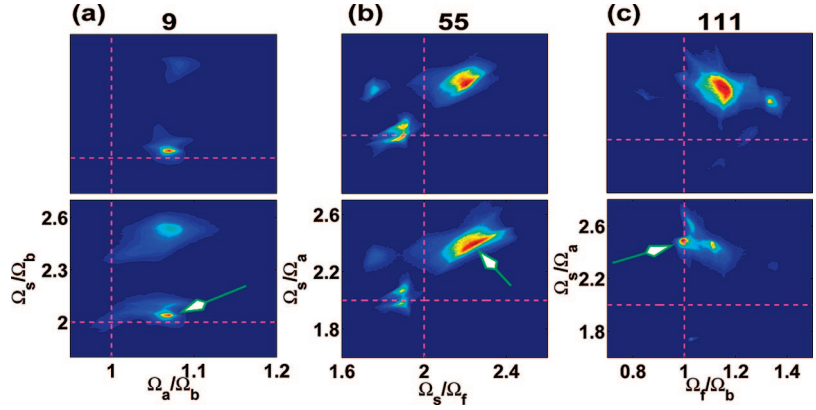

Figure 6. Phase space representations for the select eigenstates of CDBrClF belonging to polyad $N = 5$. In all the plots the density varies from being a maximum (red) to minimum (blue). The top panels, with axes and ranges identical to the bottom panels, represent the (E_α, N) web. The corresponding bottom panels show the eigenstates $|\alpha\rangle$ lifted onto the web using the procedure described in section 3.2. The (E_α, N) web is constructed using 2500 trajectories propagated to $T = 10$ ps. Some of the primary resonances (dotted magenta line) and enhanced densities (green arrows) are shown for clarity. (a) State 9 shows enhanced intensity closer to the $\Omega_s \approx 2\Omega_b$ Fermi resonance. (b) State 55 shows several regions of enhanced density with the (E_α, N) and lifted eigenstate plots being very similar. (c) State 111 clearly shows enhanced density, in contrast to the (E_α, N) plot, corresponding to the $\Omega_f \approx \Omega_b$ induced resonance.

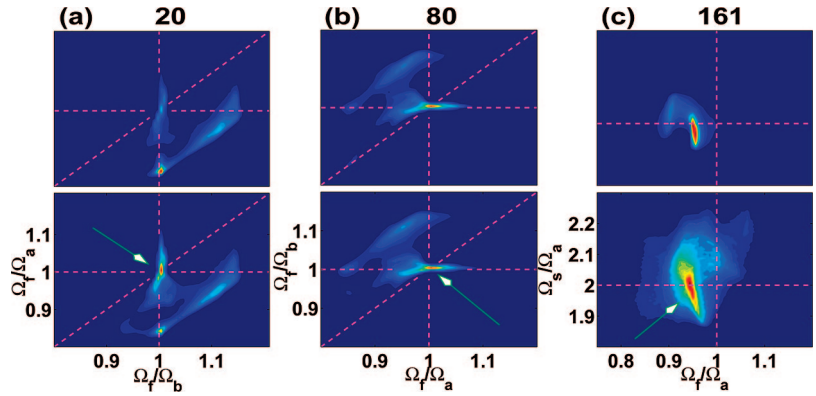

Figure 7. Same as in Figure 6 for the select eigenstates of CF_3CHFI belonging to polyad $N = 5$. (a) State 20 shows enhanced intensity closer to the $\Omega_f \approx \Omega_a$ resonance despite the dominance of $\Omega_f \approx \Omega_b$ in the (E_α, N) plot. (b) State 80 shows simultaneous locking $\Omega_f \approx \Omega_a \approx \Omega_b$ with the lifted state and the (E_α, N) being nearly identical. (c) State 161 clearly shows enhanced density corresponding to the $\Omega_s \approx 2\Omega_a$ Fermi resonance.

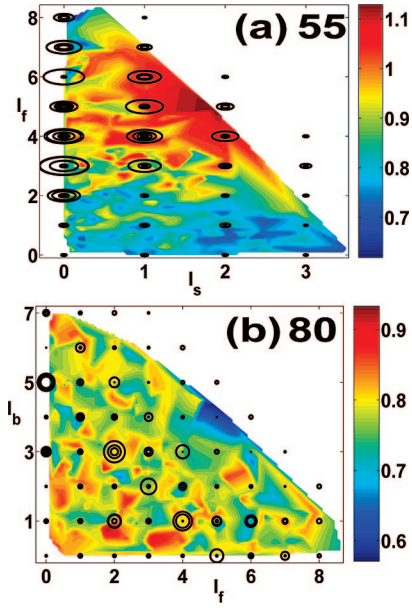

Figure 8. Quantum states 55 (a) and 80 (b) projected onto the (I_s, I_f) and (I_f, I_b) state spaces, respectively. State 55 is delocalized in the large diffusion region whereas the delocalized state 80 ignores the classical regions of high/low diffusion. These observations hold in any of the two-dimensional state space projections.

any of the relevant resonance strengths. Thus, the complexity of state 55 must be entirely classical in origin as compared to the predominantly quantum origins of the complexity of state 80.

Further insights into the differing nature of the two mixed states can be obtained by inspecting the corresponding state space representations. In panels a and b of Figure 8 the respective state spaces with classical diffusion information are shown. It is immediately clear that state 55 is delocalized in the high diffusion region of the state space whereas state 80, also delocalized, seems to largely ignore the classical template. This lends support to conjecture that the state space nature of state 80, in contrast to that of state 55, is symptomatic of mixing due to quantum mechanisms.

In the case of the mixed state 80 Figure 7b shows that the (E_α, N) web and the lifted eigenstate plot are identical with maximal density near the resonance junction $\Omega_f \approx \Omega_a \approx \Omega_b$. A crucial point to be noted here is that despite the identical nature of the lifted eigenstate plots for state 20 and state 80 there is an important difference—the (E_α, N) webs are distinct and the density shift observed for state 20 is absent in case of state 80. One possibility is to look for the appropriate frequency ratio space wherein a significant rearrangement of density occurs in going from the (E_α, N) web to the lifted eigenstate. In the case of state 80 we find that significant density changes happen in the $(\Omega_f/\Omega_a, \Omega_s/\Omega_a)$ space. Combined with the fact that the quantum expectation V_{fa}^{80} exhibits the largest deviation from the classical ergodic estimate, one can infer that the $\Omega_f \approx \Omega_a$ resonance is playing an important role. It also follows that state 80 is a highly mixed state but not an ergodic state. At this point, although our observations agree with those of the previous authors, we do not have further insights into the nature of state 80. We suspect that, due to the multistate avoided crossings, dynamical tunneling might be the cause of extensive mixing.

On the other hand, the nature of state 55 can be ascertained based on the classical resonance web. Figure 6b shows a moderate density around the $\Omega_s \approx 2\Omega_a$ Fermi resonance. However, the maximum density is away from any of the primary resonances. Similar observations hold for any choice of the frequency ratio space and clearly point to the mixed nature of the state. As mentioned before, there is scant evidence to blame avoided crossings for the observed mixing. In order to understand the mechanism of mixing, Figure 9 compares two different representations of the state. In Figure 9b we show the semiclassical angle space density representation in the $\psi_a = \psi_b$ plane. Note that the high density regions seem to be almost circular in nature. A few other states also show similar features. In comparison, Figure 9a shows the lifted eigenstate on the $(\Omega_a/\Omega_f, \Omega_s/\Omega_f)$ plane. In this representation of the phase space, different from the one in Figure 6b, it is still true that the (E_α, N) web and the lifted state are similar. Again, the maximum density does not obviously correspond to any of the primary resonances shown in Figure 9a. However, analyzing the dynamics corresponding to the maximum density regions indicated frequency lockings (1−2 ps)

$$\Omega_s - (\alpha + 2)\Omega_f + \alpha\Omega_a \approx 0 \qquad (30)$$

with $\alpha = 1, 2, 3, 4$. These resonances, shown in Figure 9a, emanate from the $(\Omega_f/\Omega_a, \Omega_s/\Omega_f) = (1/1, 2/1)$ rational point and seem to correspond well with the maximum density regions. In fact, evidence for these resonances can be found in Figure 9b as well by recognizing that some of the maximum density regions correspond to $\alpha\psi_a \approx (\alpha + 2)\psi_f$ which, using the canonical transformation, are nothing but the resonances in eq 30. It is reasonable to expect that the resonances in eq 30 are induced by the strong primary resonances. Interestingly, such examples of diffusion over an extended surface in the frequency plane have been given before by Laskar.[77] The results of Figure

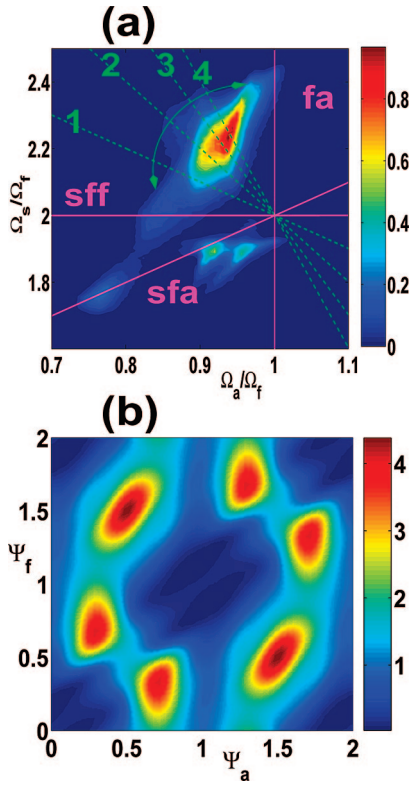

Figure 9. Two different representations of the CDBrClF mixed state 55. (a) Eigenstate lifted onto the $(\Omega_a/\Omega_f, \Omega_s/\Omega_f)$ space. Key primary resonances are shown as magenta lines and labeled. Some of the higher order induced resonances are shown as green lines and labeled by the value of α in eq 30. (b) Eigenstate density $|\Psi(\psi)|^2$ in the $\psi_a = \psi_b$ plane. Note the circular regions of high density which correspond to the high-density region in (a). See text for discussion.

9, to the best of our knowledge, represent a first example of the impact of extended diffusion on the quantum eigenstates. Thus state 55 is a mixed multimode state and an instance of dynamical decoupling which is hard to decipher from purely quantum approaches. It is also worth emphasizing that Pearman and Gruebele[83] and Leitner and Wolynes[84] have stressed the importance of higher order anharmonic coupling to long time IVR. Figure 9 demonstrates the crucial role played by high order nonlinear resonances in determining the nature of mixed eigenstates.

6. Conclusions

In this work we have shown that it is possible to extend the classical-quantum correspondence based approaches to provide dynamical assignments for systems with three or more degrees of freedom. The utility of quantum expectation values of the various resonance operators (level velocities) in identifying sequences of localized states has been demonstrated in the molecular context. In this regard the knowledge of the level-velocity values in the classically ergodic and the classically integrable limits aid in the eigenstate assignments. Since the examples considered in the present work represent realistic, nonscaling molecular systems, the success of our approach augurs well for analyzing eigenstates in dynamically interesting energy regions of larger molecules with substantial density of states. We remark here that a large density of states does not automatically imply that every state is highly mixed in the energy range of interest. On the contrary, based on several works, including the present one, and given the current understanding of the scaling of coupling constants, one expects to find a complex intermingling of localized and delocalized states. Such interleaving of localized and delocalized states effects the intramolecular dynamics in a profound way and our results indicate that techniques[81,82] based on level velocities should be ideal for gaining detailed insights into the dynamics.

We have also supported the level-velocity analysis and predictions by using a novel method to lift the quantum eigenstates onto the dynamical classical resonance web. It is possible to provide more refined criteria for the lifting process, but at the cost of considerable computational overhead. Efforts are currently being made in our group to come up with efficient ways to lift the quantum eigenstate onto the classical resonance web. More importantly, note that the level-velocity and the eigenstate lifting are both basis-independent methods. The results of Figures 6, 7, and 9 illustrate the central role played by the dynamical Arnol'd web in the process of IVR. There has been a concerted effort[69,70] over the last couple of years to highlight the importance of the dynamical Arnol'd web and the current work shows its utility in the context of highly excited eigenstates. It is possible, for example, to identify whether the nature of a mixed eigenstate is primarily due to classical or quantum mechanisms. Note that valuable insights are obtained even by retaining only, hence the apparent sparse nature of the resonance webs, the maximum frequency components in the wavelet transform. Although computationally demanding, there are reasons to expect that including some of the subdominant frequencies can lead to information on the role of high order resonances in terms of long time IVR dynamics and consequently into the nature of the eigenstates.

It is useful to make a couple of brief comments at this stage to compare our approach to the previous approaches based on analyzing the stabilty and bifurcations of the various periodic orbits. The periodic orbit based methods are ideally suited for systems with two or lower degrees of freedom wherein the global phase space can be easily visualized.[1] Consequently, the nature of the eigenstates can be established by lifting them into the phase space using the Wigner or the Husimi representations. However, such approaches are not practical for systems with three or more degrees of freedom, i.e., those considered in this work. Apart from the practical limitations, note that there are also conceptual issues related to the dimensionality of the phase space structures required for a clean partitioning of the phase space into dynamically distinct regions. Such partitioning is key for an unambiguous dynamically assignment of the quantum states. Thus, although the primary periodic orbits of the full four mode Hamiltonian in eq 20 can be determined via the fixed points of the flow corresponding to the reduced Hamiltonian of eq 24, these periodic orbits do not partition the phase space into dynamically distinct regions.[4] In particular, one needs to determine the higher dimensional analog known as normally hyperbolic invariant manifold (NHIM), and we refer the interested reader to the earlier literature wherein detailed discussions regarding the issues involved in computing the NHIMs are provided.[85] In the present approach an approximate partitioning is obtained by constructing the Arnol'd web which allows us, together with the level-velocity analysis, to identify interesting class of states as in Figure 9. Note that periodic orbit based techniques cannot identify such states for reasons stated above. It remains to be seen if the NHIMs are capable of revealing the existence of such partially localized states in a straightforward manner.

Clearly, unraveling the nature of the eigenstates and decoding the dynamical information requires a combination of different approaches. For instance, preceding the computationally easy

approach of Jung et al. with IPR and level-velocity calculations will lead to a more comprehensive understanding of the states and, hopefully, to much firmer dynamical assignments. While techniques like the Arnol'd web and eigenstate lifts are more involved, they do yield detailed insights and are presumably less difficult to implement as compared to the task of mapping out the NHIMs in multimode systems. Further studies are required to find the ideal mix of methods to adopt for the dynamical assignments and identify the birth of new modes due to a variety of bifurcations. Nevertheless, we believe that one now has a decent set of tools to understand the nature of the highly excited quantum states from a classical-quantum correspondence point of view.

References and Notes

(1) Kellman, M. E. *Annu. Rev. Phys. Chem.* **1995**, *46*, 395. Lu, Z.; Kellmam, M. E. *Chem. Phys. Lett.* **1995**, *247*, 195. Svitak, J.; Li, Z. M.; Rose, J.; Kellman, M. E. *J. Chem. Phys.* **1995**, *102*, 4340. Lu, Z.; Kellman, M. E. *J. Chem. Phys.* **1997**, *107*, 1. Rose, J. P.; Kellman, M. E. *J. Chem. Phys.* **1996**, *105*, 10743. Rose, J. P.; Kellman, M. E. *J. Chem. Phys.* **1996**, *105*, 7348. Kellman, M. E.; Rose, J. P.; Tyng, V. *Eur. Phys. J. D* **2001**, *14*, 225. Kellman, M. E.; Tyng, V. *Acc. Chem. Res.* **2007**, *40*, 243.

(2) Ezra, G. S. *Adv. Classical Trajectory Methods* **1992**, *1*, 1. Ezra, G. S. *Adv. Classical Trajectory Methods* **1998**, *3*, 35.

(3) Gomez Llorente, J. M.; Pollak, E. *Annu. Rev. Phys. Chem.* **1992**, *43*, 91. Frantos, S. C. *Int. Rev. Phys. Chem.* **1996**, *15*, 345.

(4) Keshavamurthy, S.; Ezra, G. S. *Chem. Phys. Lett.* **1996**, *259*, 81. Keshavamurthy, S.; Ezra, G. S. *J. Chem. Phys.* **1997**, *107*, 156.

(5) Jacobson, M. P.; Jung, C.; Taylor, H. S.; Field, R. W. *J. Chem. Phys.* **1999**, *111*, 600. Jung, C.; Taylor, H. S.; Jacobson, M. P. *J. Phys. Chem. A* **2001**, *105*, 681. Jung, C.; Ziemniak, E.; Taylor, H. S. *J. Chem. Phys.* **2001**, *115*, 2499. Waalkens, H.; Jung, C.; Taylor, H. S. *J. Phys. Chem. A* **2002**, *106*, 911. Jung, C.; Taylor, H. S.; Atilgan, E. *J. Phys. Chem. A* **2002**, *106*, 3092.

(6) Rueda, J.; Jung, C. *Mol. Phys.* **2006**, *104*, 1353. Diaz, A.; Jung, C. *Mol. Phys.* **2008**, *106*, 787.

(7) Jung, C.; Mejia-Monasterio, C.; Taylor, H. S. *J. Chem. Phys.* **2004**, *120*, 4194.

(8) Jung, C.; Mejia-Monasterio, C.; Taylor, H. S. *Phys. Chem. Chem. Phys.* **2004**, *6*, 3069.

(9) Jung, C.; Taylor, H. S.; Sibert, E. L. *J. Phys. Chem. A* **2006**, *110*, 5317.

(10) Jung, C.; Taylor, H. S. *J. Phys. Chem. A* **2007**, *111*, 3047.

(11) Martens, C. C. *J. Stat. Phys.* **1992**, *68*, 207.

(12) Wu, G. Z. *Chem. Phys. Lett.* **1998**, *292*, 369. Ji, Z. Q.; Wu, G. Z. *Chem. Phys. Lett.* **2000**, *319*, 45. Wang, P. J.; Wu, G. Z. *Chem. Phys. Lett.* **2003**, *371*, 238. Wang, H. R.; Wang, P. J.; Wu, G. Z. *Chem. Phys. Lett.* **2004**, *399*, 78. Huang, J.; Wu, G. Z. *Chem. Phys. Lett.* **2007**, *439*, 231.

(13) Keshavamurthy, S. *J. Phys. Chem. A* **2001**, *105*, 2668. Semparithi, A.; Charulatha, V.; Keshavamurthy, S. *J. Chem. Phys.* **2003**, *118*, 1146. Semparithi, A.; Keshavamurthy, S. *Phys. Chem. Chem. Phys.* **2003**, *5*, 5051. Semparithi, A.; Keshavamurthy, S. *Chem. Phys. Lett.* **2004**, *395*, 327.

(14) Davis, M. J. *J. Phys. Chem.* **1988**, *92*, 3124. Davis, M. J. *Chem. Phys. Lett.* **1992**, *192*, 479. Davis, M. J. *Int. Rev. Phys. Chem.* **1995**, *14*, 15. Davis, M. J. *J. Chem. Phys.* **1997**, *107*, 4507.

(15) Atkins, K. M.; Logan, D. E. *J. Chem. Phys.* **1992**, *97*, 2438. Atkins, K. M.; Logan, D. E. *Phys. Lett. A* **1992**, *162*, 255.

(16) Zhilinskii, B. *Chem. Phys.* **1989**, *137*, 1. Sadovskii, D. A.; Zhilinskii, B. *Phys. Rev. A* **1993**, *48*, 1035. Zhilinskii, B. *Spectrochim. Acta, Part A* **1996**, *52*, 881. Kozin, I. N.; Sadovskii, D.; Zhilinskii, B. I. *Spectrochim. Acta, Part A* **2005**, *61*, 2867.

(17) Siebert, E. L., III.; McCoy, A. B. *J. Chem. Phys.* **1996**, *109*, 2111.

(18) Ishikawa, H.; Field, R. W.; Farantos, S. C.; Joyeux, M.; Koput, J.; Beck, C.; Schinke, R. *Annu. Rev. Phys. Chem.* **1999**, *50*, 443. Weiss, J.; Hauschildt, J.; Grebenshchikov, S. Y.; Duren, R.; Schinke, R.; Koput, J.; Stamatiadis, S.; Farantos, S. C. *J. Chem. Phys.* **2000**, *112*, 77. Joyeux, M.; Farantos, S. C.; Schinke, R. *J. Phys. Chem. A* **2002**, *106*, 5407. Azzam, T.; Schinke, R.; Farantos, S. C.; Joyeux, M.; Peterson, K. A. *J. Chem. Phys.* **2003**, *118*, 9643.

(19) Vanroosmalen, O. S.; Iachello, F.; Levine, R. D.; Dieperink, A. E. L. *J. Chem. Phys.* **1983**, *79*, 2515. Iachello, F.; Oss, S. *J. Chem. Phys.* **1996**, *104*, 6956. Sako, T.; Yamanouchi, K.; Iachello, F. *J. Chem. Phys.* **2002**, *117*, 1641. Iachello, F.; Perez-Bernal, F. *Mol. Phys.* **2008**, *106*, 223.

(20) Child, M. S. *J. Mol. Spectrosc.* **2001**, *210*, 157.

(21) Einstein, A. *Ver. Dtsch. Phys. Ges.* **1917**, *19*, 82. Brillouin, L. *J. Phys. (Paris)* **1926**, *7*, 353. Keller, J. *Ann. Phys.* **1958**, *4*, 180.

(22) Heller, E. J. *Phys. Rev. Lett.* **1984**, *53*, 1515.

(23) Shirts, R. B.; Reinhardt, W. P. *J. Chem. Phys.* **1982**, *77*, 5204.

(24) Wisniacki, D. A.; Vergini, E.; Benito, R. M.; Borondo, F. *Phys. Rev. Lett.* **2005**, *94*, 054101. Borondo, F.; Vergini, E.; Wisniacki, D. A.; Zembekov, A. A.; Benito, R. M. *J. Chem. Phys.* **2005**, *122*, 111101. Sibert, E. L.; Vergini, E.; Benito, R. M.; Borondo, F. *New J. Phys.* **2008**, *10*, 053016.

(25) Bacic, Z.; Light, J. C. *Annu. Rev. Phys. Chem.* **1989**, *40*, 469. Ribeiro, F.; Iung, C.; Leforestier, C. *J. Theor. Comput. Chem.* **2003**, *2*, 609. Carrington, T. *Can. J. Chem.* **2004**, *82*, 900. Iung, C.; Ribeiro, F.; Sibert, E. L. *J. Phys. Chem. A* **2006**, *110*, 5420. Christiansen, O. *Phys. Chem. Chem. Phys.* **2007**, *9*, 2942. Pasin, G.; Iung, C.; Gatti, F.; Meyer, H. D. *J. Chem. Phys.* **2007**, *126*, 024302. Yagi, K.; Hirata, S.; Hirao, K. *Phys. Chem. Chem. Phys.* **2008**, *10*, 1781.

(26) For reviews spanning nearly three decades see. Smalley, R. E. *Annu. Rev. Phys. Chem.* **1983**, *34*, 129. Hamilton, C. E.; Kinsey, J. L.; Field, R. W. *Annu. Rev. Phys. Chem.* **1986**, *37*, 493. Quack, M. *Annu. Rev. Phys. Chem.* **1990**, *41*, 839. Uzer, T. *Phys. Rep.* **1991**, *199*, 73. Lehmann, K. K.; Scoles, G.; Pate, B. H. *Annu. Rev. Phys. Chem.* **1994**, *45*, 241. Nesbitt, D. J.; Field, R. W. *J. Phys. Chem.* **1996**, *100*, 12735. Crim, F. F. *J. Phys. Chem.* **1996**, *100*, 12725. Leitner, D. M.; Wolynes, P. G. *ACH—Models Chem.* **1997**, *134*, 663. Gruebele, M.; Bigwood, R. *Int. Rev. Phys. Chem.* **1998**, *17*, 91. Leitner, D. M. *Int. J. Quantum Chem.* **1999**, *75*, 523. Keske, J. C.; Pate, B. H. *Annu. Rev. Phys. Chem.* **2000**, *51*, 323. Nordholm, S.; Bäck, A. *Phys. Chem. Chem. Phys.* **2001**, *3*, 2289. Callegari, A.; Rizzo, T. R. *Chem. Soc. Rev.* **2001**, *30*, 214. Bar, I.; Rosenwaks, S. *Int. Rev. Phys. Chem.* **2001**, *20*, 711. Grebenshchikov, S. Yu.; Schinke, R.; Hase, W. L. In *Comprehensive Chemical Kinetics, Part I*; Green, N. J. B., Ed.; Elsevier: Amsterdam, 2003; Vol. 39,Chapter 3. Assman, J.; Kling, B.; Abel, B. *Angew. Chem., Int. Ed.* **2003**, *42*, 2226. Gruebele, M.; Wolynes, P. G. *Acc. Chem. Res.* **2004**, *37*, 261. Carpenter, B. K. *Annu. Rev. Phys. Chem.* **2005**, *56*, 57. Elles, C. G.; Crim, F. F. *Annu. Rev. Phys. Chem.* **2006**, *57*, 273. Leitner, D. M. *Annu. Rev. Phys. Chem.* **2008**, *59*, 233.

(27) Jacobson, M. P.; Field, R. W. *J. Phys. Chem. A* **2000**, *104*, 3073. Field, R. W.; O'Brien, J. P.; Jacobson, M. P.; Solina, S. A. B.; Polik, W. F.; Ishikawa, H. *Adv. Chem. Phys.* **1997**, *101*, 463.

(28) Quack, M. *J. Mol. Struct.* **1995**, *347*, 245. Marquardt, R.; Quack, M. *Encyclopedia of Chemical Physics and Physical Chemistry I*; Moore, J. H., Spencer, N. D., Eds.; IOP: Bristol, 2001; p 897. Quack, M.; Stohner, J.; Willeke, M. *Annu. Rev. Phys. Chem.* **2008**, *59*, 741.

(29) Beil, A.; Hollenstein, H.; Monti, O. L. A.; Quack, M.; Stohner, J. *J. Chem. Phys.* **2000**, *113*, 2701.

(30) Pochert, J.; Quack, M.; Stohner, J.; Willeke, M. *J. Chem. Phys.* **2000**, *113*, 2719.

(31) Cushman, R. H.; Duistermaat, J. J. *Bull. Am. Math. Soc.* **1988**, *19*, 475. Joyeux, J.; Sadovskii, D. A.; Tennyson, J. *Chem. Phys. Lett.* **2003**, *382*, 439. Cooper, C. D.; Child, M. S. *Phys. Chem. Chem. Phys.* **2005**, *7*, 2731.

(32) Davis, M. J.; Heller, E. J. *J. Chem. Phys.* **1981**, *75*, 246. Heller, E. J. *J. Phys. Chem.* **1995**, *99*, 2625. Heller, E. J. *J. Phys. Chem. A* **1999**, *103*, 10433.

(33) Keshavamurthy, S. *J. Chem. Phys.* **2003**, *119*, 161. Keshavamurthy, S. *J. Chem. Phys.* **2005**, *122*, 114109. Keshavamurthy, S. *Phys. Rev. E* **2005**, *72*, 045203(R). Keshavamurthy, S. *Int. Rev. Phys. Chem.* **2007**, *26*, 521.

(34) Sundberg, R. L.; Abramson, E.; Kinsey, J. L.; Field, R. W. *J. Chem. Phys.* **1985**, *83*, 466.

(35) Sitja, G.; Pique, J. P. *Phys. Rev. Lett.* **1994**, *73*, 232.

(36) Keske, J.; McWhorter, D. A.; Pate, B. H. *Int. Rev. Phys. Chem.* **2000**, *19*, 363.

(37) Leitner, D. M.; Gruebele, M. *Mol. Phys.* **2008**, *106*, 433.

(38) Annesley, C. J.; Berke, A. E.; Crim, F. F. *J. Phys. Chem. A* **2008**, *112*, 9448.

(39) Dunham, J. L. *Phys. Rev.* **1932**, *41*, 721.

(40) Joyeux, M.; Sugny, D. *Can. J. Phys.* **2002**, *80*, 1459.

(41) McCoy, A. B.; Sibert, E. L. In *Computational Molecular Spectroscopy*; Jensen, P., Bunker, P. R., Eds.; Wiley: Chichester, U.K., 2000.

(42) Van Vleck, J. H. *Rev. Mod. Phys.* **1951**, *23*, 213.

(43) Birkhoff, G. D. *Dynamical Systems, Colloq. Pub. No. 9, revised edition*; American Mathematical Society: Providence, RI, 1979.

(44) Gustavson, F. G. *Astron. J.* **1966**, *71*, 670.

(45) Kellman, M. E. *J. Chem. Phys.* **1990**, *93*, 6630.

(46) Fried, L. E.; Ezra, G. S. *J. Chem. Phys.* **1987**, *86*, 6270.

(47) Lefebvre-Brion, H.; Field, R. W. *The Spectra and Dynamics of Diatomic Molecules*; Elsevier: Amsterdam, 2004.

(48) Kuzmin, M. V.; Nemov, I. V.; Stuchebrukhov, A. A.; Bagratashvili, V. N.; Letokhov, V. S. *Chem. Phys. Lett.* **1986**, *124*, 522. Kuzmin, M. V.; Stuchebrukhov, A. In *Laser Spectroscopy of Highly Vibrationally Excited Molecules*; Letokhov, V. S., Ed.; Adam Hilger: Bristol, 1989.

(49) Heisenberg, W. *Z. Phys.* **1925**, *33*, 879. Translated in *Sources of Quantum Mechanics*; Van der Waerden, B. L., Ed.; Dover: Mineola, NY, 1967.

(50) Lichtenberg, A. J.; Lieberman, M. A. *Regular and Chaotic Dynamics*, 2nd ed.; Springer: Berlin, 1992.

(51) Feynman, R. P. *Phys. Rev.* **1939**, *56*, 340.

(52) Noid, D. W.; Koszykowski, M. L.; Tabor, M.; Marcus, R. A. *J. Chem. Phys.* **1980**, *72*, 6169.
(53) Ramachandran, B.; Kay, K. G. *J. Chem. Phys.* **1993**, *99*, 3659.
(54) Pechukas, P. *Phys. Rev. Lett.* **1983**, *51*, 943. Yukawa, T. *Phys. Rev. Lett.* **1985**, *54*, 1883. Nakamura, K.; Lakshmanan, M. *Phys. Rev. Lett.* **1986**, *57*, 1661. Wilkinson, M. *J. Phys. A: Math. Gen.* **1987**, *20*, 2415. Takami, T.; Hasegawa, H. *Phys. Rev. Lett.* **1992**, *68*, 419. Simons, B. D.; Altshuler, B. L. *Phys. Rev. Lett.* **1993**, *70*, 4063. Fyodorov, Y. V. *Phys. Rev. Lett.* **1994**, *73*, 2688. Zakrzewski, J.; Delande, D. *Phys. Rev. E* **1993**, *47*, 1650. Guarneri, I.; Zyckowski, K.; Zakrzewski, J.; Molinari, L.; Casati, G. *Phys. Rev. E* **1995**, *52*, 2220. Sano, M. *Phys. Rev. E* **1996**, *54*, 3591. Kuntsman, P.; Zyckowski, K.; Zakrzewski, J. *Phys. Rev. E* **1997**, *55*, 2446. Lakshminarayan, A.; Cerruti, N. R.; Tomsovic, S. *Phys. Rev. E* **1999**, *60*, 3992. Cerruti, N. R.; Keshavamurthy, S.; Tomsovic, S. *Phys. Rev. E* **2003**, *68*, 056205.
(55) Schnirelman, A. I. *Usp. Mat. Nauk* **1974**, *29*, 181. Colin de Verdiere, Y. *Commun. Math. Phys.* **1985**, *102*, 497. Zelditch, S. *Duke Math. J.* **1987**, *55*, 919.
(56) Kaplan, L.; Heller, E. J. *Physica D* **1998**, *121*, 1.
(57) Bäck, A.; Nordholm, S.; Nyman, G. *J. Phys. Chem. A* **2004**, *108*, 8782.
(58) Bäcker, A.; Schubert, R.; Stifter, P. *Phys. Rev. E* **1998**, *57*, 5425.
(59) Peres, A. *Phys. Rev. A* **1984**, *30*, 504. Feingold, M.; Moiseyev, N.; Peres, A. *Phys. Rev. A* **1984**, *30*, 509. Feingold, M.; Moiseyev, N.; Peres, A. *Chem. Phys. Lett.* **1985**, *117*, 344. Feingold, M.; Peres, A. *Phys. Rev. A* **1986**, *34*, 591.
(60) Eckhardt, B.; Fishman, S.; Keating, J.; Agam, O.; Main, J.; Müller, K. *Phys. Rev. E* **1995**, *52*, 5893.
(61) Mehlig, B.; Müller, K.; Eckhardt, B. *Phys. Rev. E* **1999**, *59*, 5272.
(62) Boosé, D.; Main, J. *Phys. Rev. E* **1999**, *60*, 2831.
(63) Jacobson, M. P.; Silbey, R. J.; Field, R. W. *J. Chem. Phys.* **1999**, *110*, 845.
(64) Roberts, F. L.; Jaffé, C. *J. Chem. Phys.* **1993**, *99*, 2495.
(65) Husimi, K. *Proc. Math. Soc. Jpn.* **1940**, *22*, 264.
(66) Wigner, E. P. *Phys. Rev.* **1932**, *40*, 749.
(67) Martens, C. C.; Davis, M. J.; Ezra, G. S. *Chem. Phys. Lett.* **1987**, *142*, 519.
(68) Tang, H.; Jang, S. M.; Zhao, M. S.; Rice, S. A. *Chem. Phys. Lett.* **1998**, *285*, 143.
(69) Semparithi, A.; Keshavamurthy, S. *J. Chem. Phys.* **2006**, *125*, 141101.
(70) Shojiguchi, A.; Li, C.-B.; Komatsuzaki, T.; Toda, M. *Laser Phys.* **2006**, *17*, 1097. Shojiguchi, A.; Li, C.-B.; Komatsuzaki, T.; Toda, M. *Phys. Rev. E* **2007**, *75*, 035204(R). Shojiguchi, A.; Li, C.-B.; Komatsuzaki, T.; Toda, M. *Phys. Rev. E* **2007**, *76*, 056205.
(71) Bach, A.; Hostettler, J. M.; Chen, P. *J. Chem. Phys.* **2005**, *123*, 021101. Bach, A.; Hostettler, J. M.; Chen, P. *J. Chem. Phys.* **2006**, *125*, 024304.
(72) Paskauskas, R.; Chandre, C.; Uzer, T. *Phys. Rev. Lett.* **2008**, *100*, 083001.
(73) Shchekinova, E.; Chandre, C.; Lan, Y.; Uzer, T. *J. Chem. Phys.* **2004**, *121*, 3471.
(74) Teramoto, H.; Komatsuzaki, T. *Phys. Rev. E* **2008**, *78*, 017202.
(75) Vela-Arevalo, L. V.; Wiggins, S. *Int. J. Bifurcation Chaos Appl. Sci. Eng.* **2001**, *11*, 1359.
(76) Chandre, C.; Wiggins, S.; Uzer, T. *Physica D* **2003**, *181*, 171.
(77) Laskar, J. *Physica D* **1993**, *67*, 257.
(78) Honjo, S.; Kaneko, K. *Adv. Chem. Phys.* **2005**, *130*, 437.
(79) Ding, M. Z.; Bountis, T.; Ott, E. *Phys. Lett. A* **1990**, *151*, 395. Perry, A. D.; Wiggins, S. *Physica D* **1994**, *71*, 102. Tsiganis, K.; Anastasiadis, A.; Varvoglis, H. *Chaos, Solitons Fractals* **2000**, *11*, 2281. Zaslavsky, G. M. *Physica D* **2002**, *168*, 292. Sun, Y. S.; Zhou, L. Y.; Zhou, J. L. *Celest. Mech. Dyn. Astron.* **2005**, *92*, 257. Bunimovich, L. A. *Nonlinearity* **2008**, *21*, T13.
(80) Schofield, S.; Wolynes, P. G. *J. Chem. Phys.* **1993**, *98*, 1123. Schofield, S.; Wolynes, P. G. *J. Phys. Chem.* **1995**, *99*, 2753. Wong, V.; Gruebele, M. *J. Phys. Chem. A* **1999**, *103*, 10083.
(81) Keshavamurthy, S.; Cerruti, N. R.; Tomsovic, S. *J. Chem. Phys.* **2002**, *117*, 4168.
(82) Jacobson, M. P.; Field, R. W. *Chem. Phys. Lett.* **2000**, *320*, 553.
(83) Pearman, R.; Gruebele, M. *J. Chem. Phys.* **1998**, *108*, 6561.
(84) Leitner, D. M.; Wolynes, P. G. *J. Chem. Phys.* **1996**, *105*, 11226.
(85) Wiggins, S. *Normally Hyperbolic Invariant Manifolds in Dynamical Systems*; Springer: Berlin, 1994. Gillilan, R. E.; Ezra, G. S. *J. Chem. Phys.* **1991**, *94*, 2648. Begie, D. *Chaos, Solitons Fractals* **1995**, *5*, 177.

JP807231P